JNeurosci
THE JOURNAL OF NEUROSCIENCE

Research Articles | Development/Plasticity/Repair

Dysfunction of Unc119, a transducin-binding protein, leads to cone-rod dystrophy through activating JAK-STAT and NF-κB inflammatory pathways in the mouse retina

https://doi.org/10.1523/JNEUROSCI.2245-24.2025

Received: 26 November 2024
Revised: 3 October 2025
Accepted: 13 October 2025

Copyright © 2025 the authors

This Early Release article has been peer reviewed and accepted, but has not been through the composition and copyediting processes.The final version may differ slightly in style or formatting and will contain links to any extended data.

Alerts: Sign up at www.jneurosci.org/alerts to receive customized email alerts when the fully formatted version of this article is published.

Dysfunction of Unc119, a transducin-binding protein, leads to cone-rod dystrophy through activating JAK-STAT and NF-κB inflammatory pathways in the mouse retina

Abbreviated title: Unc119 mechanism in retinal cone-rod dystrophy

Koki Kobayashi[1], Taro Chaya[1], Hung-Ya Tu[1], Yamato Maeda[1], Yuki Nakashima[1], Ryotaro Tsutsumi[1], Haruka Yamamoto[1], Toshinori Tsujii[1], Daisuke Okuzaki[2], Takahisa Furukawa[1,*]

[1]Laboratory for Molecular and Developmental Biology, Institute for Protein Research, The University of Osaka, Osaka, 565-0871, Japan

[2]Genome Information Research Center, Research Institute for Microbial Diseases, The University of Osaka, Osaka 565-0871, Japan

[*]Author for correspondence

Takahisa Furukawa

E-mail: takahisa.furukawa@protein.osaka-u.ac.jp

Laboratory for Molecular and Developmental Biology, Institute for Protein Research, Osaka University, 3-2 Yamadaoka, Suita, Osaka, 565-0871, Japan

Phone: +81-6-6879-8631

Fax: +81-6-6879-8633

Number of pages: 51

Number of figures: 7

JNeurosci Accepted Manuscript

Number of tables: 1

Number of multimedia: 0

Number of 3D models: 0

Number of words: abstract (234), significance statement (119), introduction (596), discussion (1305)

Conflict of interest

The authors declare that they have no conflicts of interest.

Acknowledgements

We thank U. Nakagawa for LC-MS/MS analysis, M. Kadowaki, M. Wakabayashi, Y Kinooka, N. Nakashima, and T. Kaneko for technical assistance, and Editage for English language editing. This work was supported by Grant-in-Aid for Scientific Research (21H02657, 24K09996) and Grant-in-Aid for Challenging Research (Exploratory) (23K18199) from the Japan Society for the Promotion of Science, AMED-CREST (21gm1510006) from the Japan Agency for Medical Research and Development, Japan Science and Technology Agency (JST) Moonshot R&D (JPMJMS2024), JST COI-NEXT (JPMJPF2018), OU Master Plan Implementation Project, and the Takeda Science Foundation.

JNeurosci Accepted Manuscript

Abstract

Transducin is a heterotrimeric G protein that is a component of the phototransduction cascade in rod and cone photoreceptor cells of the retina. Gnat1, a rod-specific transducin α-subunit, regulates light/dark adaptation by changing its subcellular localization depending on light. Our previous study revealed that Gnat1 translocation in rod photoreceptor cells under light/dark conditions requires E3 ligase Klhl18-mediated ubiquitination and degradation of Unc119, a Gnat1-binding protein. A mutation in the human *UNC119* gene is associated with cone-rod dystrophy (CRD); however, the underlying pathological mechanism remains unclear. In this study, we generated and analyzed *Unc119*-deficient (*Unc119*$^{-/-}$) mice. We found that the retinas of *Unc119*$^{-/-}$ mice of both sexes exhibited progressive photoreceptor degeneration, resembling CRD in humans. We also found that Unc119 interacts with Gnat2 in cone photoreceptor cells and that Unc119 is essential for the translocation of Gnat2 to the outer segment in cone photoreceptor cells. RNA-seq and subsequent bioinformatics analysis revealed the predicted activation of the JAK-STAT and NF-κB pathways in the *Unc119*$^{-/-}$ retina. Treatment of *Unc119*$^{-/-}$ mice with curcumin, an inhibitor of the JAK-STAT and NF-κB pathways, suppressed inflammation and cone photoreceptor cell degeneration in *Unc119*$^{-/-}$ retinas. Furthermore, a human CRD associated-*UNC119* mutant protein competitively inhibited the interaction between UNC119 and GNAT1 or GNAT2. Taken together, the current study suggests that UNC119 dysfunction leads to CRD by affecting the JAK-STAT and NF-κB pathways, and may advance our understanding of the pathological mechanisms of CRD.

JNeurosci Accepted Manuscript

Significance Statement

Unc119 functions in light-dark adaptation by modulating the subcellular localization of transducin, a phototransduction G-protein, in rod photoreceptor cells. A human *UNC119* gene mutation is associated with cone-rod dystrophy (CRD), manifesting as cone degeneration followed by rod degeneration; however, the underlying pathological mechanism remains unclear. In this study, we found that *Unc119*-deficienct mouse retina exhibited progressive photoreceptor cell degeneration, resembling CRD. JAK-STAT and NF-κB inflammatory pathways were activated in the *Unc119*$^{-/-}$ retina, and treatment of *Unc119*$^{-/-}$ mice with curcumin, an inhibitor of JAK-STAT and NF-κB pathways, suppressed cone photoreceptor degradation. Furthermore, a human CRD-associated *UNC119* mutant protein competitively inhibited the interaction between UNC119 and a transducin component. This study advances our understanding of the pathological mechanisms that underlie CRD.

JNeurosci Accepted Manuscript

Introduction

Unc119 was initially identified as a causative gene for *Caenorhabditis elegans* (*C.elegans*) mutants associated with reduced motility, feeding behavior, and chemosensation in this organism (Maduro and Pilgrim, 1995). *Unc119* is evolutionarily conserved across species, from *C. elegans* to mice and humans, whose homologs are referred to as *Mrg4* and *HRG4*, respectively (Higashide et al., 1996; Ishiba et al., 2007). *Unc119* is notably expressed in photoreceptor cells of the retina (Swanson et al., 1998; Higashide et al., 1998) and is also present in T lymphocytes, leukocytes (eosinophils), lung fibroblasts, adrenal glands, cerebellum, and kidney (Gorska et al., 2004; Vepachedu et al., 2009; Swanson et al., 1998). Unc119 interacts with Gnat1, a rod-specific transducin α-subunit, in rods (Zhang et al., 2011). N-terminal acylation of Gnat1 is essential for Gnat1 subcellular translocation in rods (Kerov et al., 2007) and for interaction with Unc119 (Zhang et al., 2011). Gnat1 relocates from the outer segment (OS) to the cell body in response to light stimulation and plays a critical role in light adaptation (Brann and Cohen, 1987; Philp et al., 1987; Whelan and McGinnis, 1988). Studies on *Unc119*-deficient mice have shown that Gnat1 localizes to both the OS and the cell body of rods, even in the dark, suggesting that Unc119 plays an essential role in regulating Gnat1 subcellular localization during light/dark adaptation (Zhang et al., 2011). In contrast, the subcellular localization of Gnat2, a cone-specific transducin α-subunit, is known to be stable in the OS under natural conditions of illumination (Lobanova et al., 2010). This indicates that cones have a different mechanism from rods in avoiding response saturation to bright light. However, the mechanism by which Gnat2 localizes to the OS has not yet been reported. Additionally, our previous study found that the light-induced subcellular localization of Gnat1 is modulated by the E3 ligase Klhl18, which ubiquitinates and degrades Unc119 (Chaya et al., 2019). Previous research showed that Unc119 localizes at the photoreceptor synapse and interacts with synaptic proteins. Unc119 facilitated glutamate release at rod synapses (Fehlhaber et al., 2023). On the other hand, the functional role of Unc119 in cones remains unclear.

Retinal neurons do not regenerate once they degenerate, leading to irreversible blindness (Gasparini et al., 2019). Retinitis pigmentosa is a representative

JNeurosci Accepted Manuscript

retinal degeneration disease in which rod degeneration develops first, followed by the secondary degeneration of cones. In contrast, CRD is a progressive disorder characterized by initial cone degeneration followed by subsequent rod degeneration. CRD presents with symptoms, such as decreased visual acuity, reading difficulties, photophobia, and dyschromatopsia. As the disease progresses and rod function declines, affected individuals may experience reduced night vision and loss of peripheral visual fields (Hamel, 2007). Approximately one in 4,000 people are affected by this disease (Tsang and Sharma, 2018). At least 48 genes, including *UNC119*, have been reported to be associated with CRD (Birtel et al., 2018). Previous studies have identified several *UNC119* mutations in patients with CRD and macular disease, including a heterozygous p.Lys57Ter (K57X) nonsense mutation (Kobayashi et al., 2000), a heterozygous p.Asp87Asn missense mutation (Huang et al., 2013), a heterozygous c.7delG (p.Val3*) frameshift mutation (de Castro-Miro et al., 2016), and a heterozygous p.Glu201Ter nonsense mutation (Zenteno et al., 2023). Transgenic mice overexpressing the K57X mutation exhibited a progressive decrease in b-wave amplitude in electroretinograms (ERGs) and thinning of the outer nuclear layer (ONL) (Kobayashi et al., 2000). However, the mechanism of preferential degeneration in cones caused by CRD associated with *UNC119* mutation remains unclear. In this study, we investigated the functional role of *Unc119* in a mouse model and the pathological mechanisms of CRD induced by *Unc119* mutations.

JNeurosci Accepted Manuscript

Materials and Methods

Animal care

All procedures conformed to the ARVO Statement for the Use of Animals in Ophthalmic and Vision Research, and the procedures were approved by the Institutional Safety Committee on Recombinant DNA Experiments (approval ID 04913) and Animal Experimental Committees of the Institute for Protein Research (approval ID R04-02-0), Osaka University, and performed in compliance with the institutional guidelines. Mice were housed in a temperature-controlled room at 22 ℃ with a 12 h light/dark cycle. Freshwater and rodent diets were always available. All animal experiments were performed with mice of either sex at postnatal day 14 (P14), 1 month of age (1 M), 6 M, or 12 M.

Generation of *Unc119*-deficient (*Unc119*$^{-/-}$) and *Nrl*$^{-/-}$ mice

Unc119$^{-/-}$ and *Nrl*$^{-/-}$ mice were generated using the CRISPR/Cas9 system. Oligo DNAs for the gRNA sequence against mouse *Unc119* and *Nrl* were cloned into the pX330 vector (Cong et al., 2013). The plasmid constructs were injected into C57/B6J fertilized eggs, which were then transferred into the uteri of pseudopregnant ICR female mice. Mutated individuals were selected using PCR and subjected to sequencing analysis. We obtained heterozygous mice with a total 65 base-pair (bp) deletion in the *Unc119* gene and heterozygous mice with a 239 bp deletion in the *Nrl* gene. *Unc119*$^{-/-}$ mice were backcrossed with Balb/c mice for more than six generations to generate Balb/c background *Unc119*$^{-/-}$ mice. The primer sequences for the gRNA expression plasmids and genotyping are listed in Table 1. The phenotypes of the *Unc119*$^{-/-}$ and *Nrl*$^{-/-}$ mice that we generated were comparable with those reported in the previous studies (Ishiba et al., 2007, Mears et al., 2001).

Cell culture and transfection

HEK293T cells (RIKEN RCB, #RCB1637) were cultured in Dulbecco's modified Eagle's medium (DMEM) containing 10% fetal bovine serum (FBS)

JNeurosci Accepted Manuscript

supplemented with penicillin (100 μg/ml) and streptomycin (100 μg/ml) at 37 °C with 5% CO_2. Transfection was performed using the calcium phosphate method 24 h after seeding the HEK293T cells. Cell lysis was performed 48 h after transfection.

Plasmid construction

The cDNA fragments of mouse *Unc119, Gnat1, Gnat2, Gnat1-G2A, Gnat2-G2A*, human *UNC119, GNAT1, GNAT2*, and *UNC119-K57X* were amplified by PCR using mouse or human retinal cDNA as a template and subcloned into pCAGGSII-3xFLAG, pCAGGSII-2xHA, and pGAGGSII-3xMyc vectors. Primer sequences used for amplification are shown in Table 1.

RT-PCR and quantitative RT-PCR (qRT-PCR) analyses

RT-PCR and qRT-PCR were performed as previously described (Tsutsumi et al., 2018). Total RNAs were isolated from mouse tissues, including the retina, cerebrum, cerebellum, brain stem, thymus, heart, lung, kidney, liver, spleen, muscle, intestine, ovary, and testis, using TRIzol RNA extraction reagent (Invitrogen). Total RNA (0.5 or 2 μg) was reverse-transcribed into cDNA using the PrimeScript RT reagent or PrimeScript II reagent (Takara). The cDNAs were used as templates for RT-PCR reactions with rTaq polymerase (Takara). qRT-PCR analysis was performed using SYBR GreenER qPCR Super Mix Universal (Invitrogen) and Thermal Cycler Dice Real Time System Single MRQ TP700 (Takara) according to the manufacturer's instructions. Quantification was conducted using the Thermal Cycler Dice Real Time System software version 2.11 (Takara). The primer sequences used for qRT-PCR analysis are listed in Table 1.

Western blotting

Western blotting was performed as previously described (Kozuka et al., 2017). HEK293T cells were washed twice with PBS and lysed in lysis buffer

JNeurosci Accepted Manuscript

supplemented with protease inhibitors (buffer A: 20 mM Tris-HCl pH 7.4, 150 mM NaCl, 1% Nonidet P-40, 1 mM EDTA, 1 mM PMSF, 2 μg/mL leupeptin, 5 μg/mL aprotinin, and 3 μg/mL pepstatin A). Mouse retinas were lysed in lysis buffer supplemented with protease inhibitors (buffer B: 20 mM Tris-HCl pH 7.4, 150 mM NaCl, 1% Nonidet P-40, 0.5 mM EDTA, 1 mM PMSF, 2 μg/mL leupeptin, 5 μg/mL aprotinin, and 3 μg/mL pepstatin A). The samples were resolved by SDS-PAGE and transferred to PVDF membranes (Millipore) using a semi-dry transfer cell (Bio-Rad). Membranes were blocked with blocking buffer (3% skim milk and 0.05% Tween 20 in Tris-buffered saline (TBS)) for 1 h and incubated with primary antibodies overnight at 4°C. The membranes were washed three times with 0.05% Tween 20 in TBS for 10 min each and then incubated with secondary antibodies for 2–5 h at room temperature. The signals were detected using Chemi-Lumi One L (Nacalai) or Pierce Western Blotting Substrate Plus (Thermo Fisher Scientific). The following primary antibodies were used: mouse anti-FLAG M2 (1:5,000, Sigma, #F1804), rat anti-HA (1:5,000, Roche, #11-867-423-001, #60789700), rabbit anti-Myc-Tag (1:5,000, MBL, #562, #056), mouse anti-α-tubulin (1:5,000, Cell Signaling Technology, #DM1A, #T9026), rabbit anti-Unc119 (1:2,500, Chaya et al., 2019), rabbit anti-GNAT2 (1:2,500, Abcam, #ab97501), and mouse anti-GST (1:5,000, Nacalai, #04559-74). The following secondary antibodies were used: horseradish peroxidase-conjugated anti-mouse IgG (1:10,000; Zymed), anti-rat IgG (1:10,000; Jackson Laboratory), anti- rabbit IgG (1:10,000; Jackson Laboratory), and anti-guinea pig IgG (1:10,000; Jackson Laboratory).

Immunofluorescence analysis of retinal sections and whole mount retinas

Immunofluorescence analysis of the retinal sections was performed as described previously (Yamamoto et al., 2020). The mouse eyes and eyecups were fixed in 4% paraformaldehyde (PFA) in PBS for 5 or 30 min at room temperature. The 30 min fixed samples were placed in 30% sucrose in PBS overnight at 4 ℃. The samples were embedded in TissueTec OCT Compound 4583 (Sakura). Frozen 20-μm sections placed on slides were dried overnight at room temperature. The tissue sections were washed three times with PBS. The

JNeurosci Accepted Manuscript

samples were then incubated with blocking buffer (5% normal donkey serum and 0.1% Triton X-100 in PBS) for 1 h at room temperature and immunostained with primary antibodies in the blocking buffer overnight at 4 ℃. After washing with PBS, the samples were incubated with fluorescent dye-conjugated secondary antibodies and DAPI (1:1,000, Nacalai Tesque) for nuclear staining. The samples were washed three times with PBS and then coverslipped with gelvatol. For whole-mount immunostaining of the retina, each retina was gently peeled off from the sclera, rinsed in PBS and fixed with 4% PFA in PBS for 30 min. After washing with PBS, the retinas were washed permeabilized by incubation in 0.1% Triton X-100 in PBS (PBST). The retinas were then immunostained with primary antibodies in PBST at 4 °C 2 overnight. Reactions with secondary antibodies in PBST were performed overnight at 4 °C. The samples were washed three times with PBST and once with PBS and then coverslipped with Fluoro-KEEPER Antifade Reagent, Non-Hardening Type with DAPI (Nacalai Tesque, # 12745-74).

The primary antibodies used in this study were as follows: mouse anti-Rhodopsin (1:1,000, Sigma, # O4886), mouse anti-Pax6 (1:500, DSHB), mouse anti-Rom1 (1:250, a kind gift from Dr. R. Molday, University of British Columbia), rabbit anti-M-opsin (1:500, Millipore, #AB5405), goat anti-S-opsin (1:500, Santa Cruz, #sc-14363 or 1:500, ROCKLAND, #600-101-MP7S), guinea pig anti-Unc119 (1:250, Chaya et al., 2019), rabbit anti-Tα (1:500, Santa Cruz, #sc-389), rabbit anti-Chx10 (1:200, Koike et al., 2007), mouse anti-Pax6 (1:500, DSHB), rabbit anti-Calbindin (1:200, Calbiochem, #PC253L), mouse anti-Ctbp2 (1:500, BD Biosciences, #612044), guinea pig anti-Rbpms (1:1,000, Millipore, #ABN1376), rabbit anti-IbaI (1:500, WAKO, #019–19741), mouse anti-S100β (1:200, Sigma, #S-2532), rabbit anti-Gnat2 (1:500, Abcam, #ab97501), rabbit anti-Arr3 (1:500 (retinal sections) or 1:1000 (whole mount), Sigma-Aldrich, #AB15282), mouse anti-GFAP (1:500, Sigma, #G3893-.2ML), rabbit anti-C1q (1:500, Abcam, #AB182451, #1006334-19), mouse anti-Socs3 (1:250, proteintech, #66797-1-IG), and rabbit anti-NF-κB p65 (1:500, Cell Signaling TECHNOLOGY, #8342). Cy3-conjugated (1:500; Jackson ImmunoResearch Laboratories) and Alexa Fluor 488-conjugated (1:500; Sigma-Aldrich)

JNeurosci Accepted Manuscript

secondary antibodies were used. The specimens were observed under a laser confocal microscope (LSM700 or LSM900, Carl Zeiss) at temperature of 22 ℃ ± 3℃ and humidity of < 65%.

ERG recordings

Electroretinograms (ERGs) were recorded as previously described (Sugita et al., 2020). Mice were adapted to the dark overnight. Mice were anesthetized by intraperitoneal injection of ketamine (100 mg/kg) and xylazine (10 mg/kg) diluted in saline (Otsuka). The pupils were dilated using topical 0.5% tropicamide and 0.5% phenylephrine HCl. ERGs responses were measured using the PuREC system with LED electrodes (Mayo Corporation). Scotopic ERGs were recorded at four stimulus intensities ranging from −4.0 to 1.0 log cd s/m^2. The mice were light-adapted for 10 min before photopic ERGs were recorded on a rod-suppressing white background of 1.3 log cd s/m^2. Photopic ERGs were recorded at four stimulus intensities ranging from −0.5 to 1.0 log cd s/m^2. Eight and four responses were averaged for the scotopic recordings (−4.0 and −3.0 log cd s/m^2, respectively). Sixteen responses were averaged for photopic recordings.

In situ hybridization

In situ hybridization was performed as previously described (Watanabe et al., 2015). Mouse embryos and eye cups were fixed overnight with 4% PFA in PBS at 4 ℃. The tissues were equilibrated in 30% sucrose in PBS overnight at 4 ℃, embedded in TissueTec OCT compound 4583 (Sakura, Japan), and frozen. Digoxigenin-labeled antisense and sense riboprobes for mouse *Unc119* were synthesized by *in vitro* transcription using 11-digoxigenin UTPs (Roche). Unc119 cDNA fragments for *in situ* hybridization probes were produced by RT–PCR using mouse retinal cDNA as a template.

Toluidine blue staining

JNeurosci Accepted Manuscript

Toluidine blue staining of retinal sections was performed as previously described (Chaya et al., 2022). The mouse eyes were fixed in 4% PFA in PBS for 5 min at room temperature. The samples were embedded in TissueTec OCT Compound 4583 (Sakura). Frozen 20-μm sections placed on slides were dried overnight at room temperature. Retinal sections were washed with PBS and stained with 0.1% toluidine blue in PBS. After washing with PBS, the slides were coverslipped and observed immediately under a microscope. The ONL and inner nuclear layer + inner plexiform layer + ganglion cell layer thicknesses were measured and quantified using the ImageJ software (National Institutes of Health).

RNA-seq

RNA-seq analysis was performed as previously described (Yoshimoto et al., 2023) with some modifications. Total RNAs from three *Unc119*$^{+/+}$ and three *Unc119*$^{-/-}$ mouse retinas at 1 M were isolated using TRIzol RNA extraction reagent (Invitrogen). Sequencing was performed on an Illumina NovaSeq 6000 platform in 101-base single-end mode. Raw reads were mapped to mouse reference genome sequences (mm10) using the TopHat ver. 2.0.13, in combination with Bowtie2 ver. 2.3.5.1 and SAMtools ver. 1.11. The number of fragments per kilobase of exon per million mapped fragments (FPKMs) was calculated using Cufflinks ver. 2.2.1. Using cut-off (fold change > 1.4, < -1.4; $p < 0.05$, unpaired t-test), heatmap visualization was conducted using the web tool Heatmapper. Gene set enrichment analysis was performed using R package clusterProfiler (Wu et al., 2021). Upstream regulator analysis was performed using IPA (Qiagen). IPA was used to predict the activated or inhibited transcription factors based on the observed differential gene expression profiles. RNA-seq analysis datasets are available in the Gene Expression Omnibus (GEO) database of NCBI (Accession Number GSE282222).

Immunoprecipitation

JNeurosci Accepted Manuscript

Immunoprecipitation assays were performed as previously described (Tsutsumi et al., 2022). HEK293T cells were cotransfected with plasmids expressing FLAG-, HA-, and Myc-tagged proteins. After 48 h of transfection, the cells were lysed in lysis buffer supplemented with protease inhibitors (20 mM Tris (hydroxymethyl) aminomethane [Tris]–HCl pH 7.5, 150 mM NaCl, 1% Nonidet P-40 [NP-40], 1 mM ethylenediaminetetraacetate [EDTA], 1 mM phenylmethylsulfonyl fluoride [PMSF], 2 μg/ml leupeptin, 5 μg/ml aprotinin, and 3 μg/ml pepstatin A). Cell lysates were incubated with an anti-FLAG M2 affinity gel (Sigma-Aldrich) overnight at 4 ℃. The beads were washed five times with wash buffer (20 mM Tris–HCl pH 7.5, 150 mM NaCl, 1% NP-40, and 1 mM EDTA) and three times with TBS, and then eluted with elution buffer (20 mM Tris–HCl pH 7.5, 150 mM NaCl, 5 mg/ml 1 × FLAG peptide) for 1 h at 4 ℃. The immunoprecipitated samples were incubated with sodium dodecyl sulfate (SDS) sample buffer for 30 min at room temperature and analyzed by western blotting.

Pull-down assay and LC-MS/MS analysis

cDNA fragments encoding full-length mouse *Unc119* were amplified by PCR and subcloned into the pGEX-4T-3 plasmid (GE Healthcare). GST-fused protein was expressed in Escherichia coli strain BL21 (DE3) and incubated with glutathione Sepharose 4B (GE Healthcare) for 3 h at 4 ℃. *Nrl*$^{+/+}$ and *Nrl*$^{-/-}$ mouse retinas were lysed in lysis buffer supplemented with protease inhibitors (20 mM Tris-HCl pH 7.4, 150 mM NaCl, 1% Nonidet P-40, 0.5 mM EDTA, 1 mM PMSF, 2 μg/mL leupeptin, 5 μg/mL aprotinin, and 3 μg/mL pepstatin A). The GST-fused proteins bound to glutathione Sepharose 4B were incubated with the retinal lysates for 3 h at 4°C, followed by five washes with wash buffer (20 mM Tris–HCl pH 7.5, 150 mM NaCl, 1% NP-40, and 1 mM EDTA) and five additional washes with TBS. The samples were then incubated with 0.1 M Glycine (pH 1.5) on ice for 1 h. Eluted samples were analyzed by western bloting or treated with trypsin and lysis endopeptidase were subjected to Orbitrap Exploris 480 (Thermo Fisher Scientific) for LC-MS/MS. The resulting data were processed using Mascot Distiller v2.8 (Matrix Science).

JNeurosci Accepted Manuscript

Drug administration

Curcumin (Sigma, #C7727) was dissolved in dimethyl sulfoxide (DMSO) at 200 mg/mL and stored at −20°C. The administration of curcumin to mice was performed as described previously (Varner et al., 2024), with some modifications. Curcumin was dissolved in DMSO (200 mg/mL) and diluted with sunflower seed oil (Sigma-Aldrich). The solvent, with or without curcumin (100 mg/kg), was administered subcutaneously to the mice daily from P21 for seven days.

Quantification and statistical analysis

Quantification of immunofluorescence images was performed by ImageJ and ZEN software (Carl Zeiss) using maximum projection images (1024 × 1024 pixels) captured by confocal microscopy with a 20x lens. Each data point indicates the average of the measurements of the four images from one mouse. Statistical analyses were performed using GraphPad Prism version 9 (GraphPad Software). Data are presented as the mean ± SD. Statistical analyses were performed using the unpaired t-test, two-way ANOVA Šídák's multiple comparisons test, or one-way ANOVA multiple comparisons test, as indicated in the figure legends. Asterisks indicate statistical significance: $*p < 0.05$, $**p < 0.01$, $***p < 0.001$, and $****p < 0.0001$.

JNeurosci Accepted Manuscript

Results

Unc119 is expressed in developing and developed photoreceptor cells

To elucidate the functional role of Unc119 in cones and the pathophysiology underlying CRD, we examined *Unc119* expression in mouse tissues. We conducted RT-PCR analysis using various tissues from 4-week-old mice and observed the ubiquitous expression of *Unc119* (Fig. 1A). Next, we investigated the expression pattern of *Unc119* in the mouse retina using *in situ* hybridization. We observed *Unc119* signals in the neuroblastic layer (NBL) and ONL, where photoreceptor cells are located, from embryonic day 17.5 (E17.5) to P14 (Fig. 1B). These observations suggest that *Unc119* is expressed in retinal photoreceptor cells during and after development.

To investigate the functional role of Unc119 in the retina, we generated *Unc119*$^{-/-}$ mice by CRISPR-Cas9 genome editing (Fig. 1C, 1D, 1E). To confirm the loss of *Unc119* expression in the retinas of *Unc119*$^{-/-}$ mice, we performed RT-PCR, western blotting, and immunofluorescence analyses. These analyses showed a complete absence of *Unc119* mRNA and protein expression in the retinas of the *Unc119*$^{-/-}$ mice (Fig. 1F, 1G, 1H). Previous studies have reported that *Unc119* deficiency leads to the mislocalization of Gnat1 to the OS and ONL under dark-adapted conditions (Zhang et al., 2011). *Unc119*$^{-/-}$ mice exhibited Gnat1 mislocalization under dark-adapted conditions at 1M (Fig. 1I, 1J).

Unc119 deficiency decreases light responses in cones

To examine the electrophysiological properties of *Unc119*$^{-/-}$ retinas, we measured ERGs under dark-adapted (scotopic) and light-adapted (photopic) conditions at 1M. Under scotopic conditions, the a-wave amplitude reflects the responses of rods, whereas the b-wave amplitude reflects the combined activity of rod and rod bipolar cells. Under photopic conditions, the a-wave amplitude

JNeurosci Accepted Manuscript

represents cone photoreceptor cell responses, and the b-wave amplitude reflects the combined activity of cone photoreceptors and cone bipolar cells. The previous study performed scotopic ERGs (Ishiba et al., 2007). We performed both scotopic and photopic ERGs in *Unc119*$^{-/-}$ mice. No significant differences were observed between *Unc119*$^{+/+}$ and *Unc119*$^{-/-}$ mice in scotopic a- and b-waves and photopic a-wave amplitudes (Fig. 2A, 2B, 2C, 2D, 2E). However, a significant decrease in photopic b-wave amplitude was observed in *Unc119*$^{-/-}$ mice (Fig. 2D, 2F). Given that Unc119 is localized at photoreceptor synapses (Higashide et al., 1998; Fehlhaber et al., 2023), we tested signal transduction from photoreceptor cells to bipolar cells by measuring the b-wave implicit time in *Unc119*$^{+/+}$ and *Unc119*$^{-/-}$ mice. We observed that the b-wave implicit time did not change significantly (Fig. 2G, 2H). These results suggest that *Unc119* deficiency leads to a decline in cone photoreceptor function but does not significantly affect rod photoreceptor function at 1M, and does not affect synaptic transmission from photoreceptors to bipolar cells.

To investigate why the photopic b-wave amplitude in *Unc119*$^{-/-}$ mice at 1M decreased, we conducted a histological analysis of retinal sections from *Unc119*$^{+/+}$ and *Unc119*$^{-/-}$ mice. Toluidine blue staining showed no significant differences in the retinal layer thickness between the two groups (Fig. 2I). Next, we performed immunofluorescence analysis using antibodies against Rhodopsin (a marker for rod outer segments), M-opsin (a marker for M-cone outer segments), and S-opsin (a marker for S-cone outer segments). Although the length of Rhodopsin and the number of M-opsin and S-opsin signals remained unchanged, mislocalization of M-opsin and S-opsin to the outer plexiform layer (OPL) was observed in the *Unc119*$^{-/-}$ retina (Fig. 2J, 2K, 2L). Mislocalization of the M-opsin and S-opsin signals to the OPL was not observed in the retina of *Unc119*$^{-/-}$ mice at P14 (Fig. S1). Immunofluorescence analysis using markers for other retinal cells, including Chx10 (bipolar cells), Pax6 (amacrine and ganglion cells), Calbindin (horizontal cells and some amacrine cells), Ctbp2 (photoreceptor synapses), Rbpms (ganglion cells), and S100β (Müller glial cells), showed no significant differences between the *Unc119*$^{+/+}$ and *Unc119*$^{-/-}$ retinas (Fig. 2M, 2N, 2O, 2P, 2Q, 2R, S2).

JNeurosci Accepted Manuscript

Unc119 deficiency causes progressive photoreceptor cell degeneration

Mutations in *UNC119* have been identified in patients with CRD (Kobayashi et al., 2000; Huang et al., 2013; de Castro-Miro et al., 2016; Zenteno et al., 2023). To determine whether *Unc119*$^{-/-}$ mice exhibited a similar pathology, we conducted ERGs and histological analyses at 6 and 12 M. While ERGs analysis showed no significant differences in scotopic b-wave and photopic a-wave amplitudes between the *Unc119*$^{+/+}$ and *Unc119*$^{-/-}$ mice at 6M, decreases in scotopic a-wave and photopic b-wave amplitudes were observed in the *Unc119*$^{-/-}$ mice (Fig. S3A, S3B, S3C, S3D, S3E, S3F). At 6M, the b-wave implicit time of ERGs in *Unc119*$^{-/-}$ mice showed no significant change compared with that in *Unc119*$^{+/+}$ mice (Fig. S3G, S3H). In the histological analysis, toluidine blue staining revealed a reduction in ONL thickness in *Unc119*$^{-/-}$ mice at 6M (Fig. S3I). Immunofluorescence analysis showed no significant change in Rhodopsin length, but displayed a decrease in the number of M-opsin-, S-opsin-, and arrestin 3 (Arr3)-positive cells, along with mislocalization of the M-opsin signals (Fig. S3J, S3K, S3L, S3M). A decrease in the number of cones was also observed in *Unc119*$^{-/-}$ mice by counting Arr3-positive OS signals using whole mount tissues (Fig. S3N). These findings suggest that cones and a part of the rods are progressively degenerated in *Unc119*$^{-/-}$ mice at 6M.

ERGs analysis at 12M revealed decreases in both scotopic a-wave and photopic b-wave amplitudes in *Unc119*$^{-/-}$ mice (Fig. 3A, 3B, 3C, 3D, 3E, 3F). The b-wave implicit time of ERGs in *Unc119*$^{-/-}$ mice was not significantly different from that in *Unc119*$^{+/+}$ mice (Fig. 3G, 3H), suggesting that *Unc119* deficiency leads to a decline in photoreceptor cell function, but does not significantly affect synaptic transmission from photoreceptor cells to bipolar cells. Toluidine blue staining revealed further thinning of the ONL in *Unc119*$^{-/-}$ mice at 12M (Fig. 3I). Immunofluorescence analysis also demonstrated reductions in the thickness of rhodopsin and in the number of M-opsin-, S-opsin-, and Arr3-positive cells (Fig. 3J, 3K, 3L, 3M). These findings suggest that *Unc119* deficiency causes progressive photoreceptor cell degeneration, resembling CRD in humans.

JNeurosci Accepted Manuscript

Unc119 interacts with Gnat2 in cones

To elucidate the functional mechanism of Unc119 in cones, we attempted to identify the interaction partners of the Unc119 protein in cones by performing a pull-down assay followed by LC-MS/MS analysis using *Nrl*$^{-/-}$ mouse retinas. *Nrl* is a transcription factor that regulates rod cell fate during development. *Nrl* deficiency causes loss of rod photoreceptor cell features and gain in cone photoreceptor cell characteristics (Swaroop et al., 1992; Mears et al., 2001). We generated *Nrl*$^{-/-}$ mice using the CRISPR/Cas9 system and performed western blotting and immunofluorescence analysis of *Nrl*$^{-/-}$ retinas using antibodies against Rhodopsin, S-opsin, M-opsin, and Unc119. The loss of Rhodopsin signal and the increase in M-opsin and S-opsin signals suggest that the *Nrl*$^{-/-}$ mice also lost the characteristics of rods and gained those of cones. We observed that the localization and expression level of Unc119 were preserved in the *Nrl*$^{-/-}$ retina compared to those in the control retina (Fig. 4A, S4). We performed pull-down assay and LC-MS/MS analysis using three types of samples: GST protein reacted with *Nrl*$^{-/-}$ retinal lysates, GST-fused mouse Unc119 (mUnc119) reacted with lysis buffer, and GST-fused mUnc119 reacted with *Nrl*$^{-/-}$ retinal lysates. We used GST protein reacted with *Nrl*$^{-/-}$ retinal lysates and GST-fused mUnc119 reacted with lysis buffer as negative controls. Using normalized total spectra, fifty-eight proteins were detected in the three types of samples; only four proteins, Gnat2, Ytdc2, Tba1a, and Hmmr, were detected specifically in GST-fused mUnc119 that reacted with *Nrl*$^{-/-}$ retinal lysates (Fig. 4B, 4C).

Among these four proteins, based on expression pattern, we focused on the G protein subunit alpha transducin 2 (Gnat2), a cone photoreceptor-specific transducin alpha subunit. The interaction between Unc119 and Gnat2 was examined by immunoprecipitation and pull-down assays (Fig. 4D, S5). In an immunoprecipitation assay, Unc119 interacted with Gnat2 as well as with Gnat1. This result suggests that Unc119 interacts with Gnat1 in rods and Gnat2 in cones. Immunofluorescence analysis with an antibody against Gnat2 was performed using *Unc119*$^{+/+}$ and *Unc119*$^{-/-}$ mouse retinas at 1M and P14.

JNeurosci Accepted Manuscript

Although the number of cone OS was not significantly different between the two groups at 1M and P14, the Gnat2 signal intensity in the OS, but not in the IS, ONL, and OPL, was reduced in the *Unc119*$^{-/-}$ retinas both at 1M and P14 (Fig. 4E, 4F, S6). To determine the expression level of Gnat2 protein, we performed western blot analysis of retinas from *Unc119*$^{+/+}$ and *Unc119*$^{-/-}$ mice at P14 using the anti-Gnat2 antibody. The Gnat2 protein expression level was not significantly different between *Unc119*$^{+/+}$ and *Unc119*$^{-/-}$ retinas (Fig. 4G), suggesting that Unc119 is required for Gnat2 localization in the OS.

N-terminal glycine (G2) acylation of Gnat1 is essential for its interaction with Unc119 and for proper subcellular localization change of Gnat1 from the cell body to the OS (Goc et al., 2008; Kerov et al., 2007). To confirm whether N-terminal glycine (G2) acylation of Gnat2 is required for its interaction with Unc119, we generated a Gnat2-G2A mutant protein, in which G2 was replaced with alanine (G2A). We conducted immunoprecipitation analysis to test whether Unc119 interacts with Gnat1-WT, Gnat1-G2A, Gnat2-WT, or Gnat2-G2A (Fig. 4H, 4I). The immunoprecipitation results showed that Unc119 interacts with both Gnat1-WT and Gnat2-WT, but not with Gnat1-G2A or Gnat2-G2A, suggesting that G2 acylation of both Gnat1 and Gnat2 is essential for the interaction with Unc119.

NF-κB and JAK-STAT pathways are activated by Unc119 deficiency in the retina

To investigate the transcriptional profile alterations of *Unc119*$^{-/-}$ retinas, we conducted RNA-seq analysis of *Unc119*$^{+/+}$ and *Unc119*$^{-/-}$ mouse retinas at 1M. We observed 80 downregulated genes and 286 upregulated genes in the *Unc119*$^{-/-}$ retina, except *Unc119* (cut-off at average fold change > 1.4 or < -1.4; $p < 0.05$) (Fig. 5A). We focused on four upregulated genes: glial fibrillary acidic protein (GFAP), complement component 1q subcomponent alpha polypeptide (C1qa), complement component 1q subcomponent beta polypeptide (C1qb), and complement component 1q subcomponent C chain (C1qc), since the upregulation of these genes is associated with glial activation and neurodegeneration (Sarthy et al., 1991; Palko et al., 2022; Jiao et al., 2018). To

JNeurosci Accepted Manuscript

determine whether the expression of these genes was altered in *Unc119* deficient retina in vivo, we immunostained retinal sections from *Unc119*$^{+/+}$ and *Unc119*$^{-/-}$ mice with antibodies against GFAP and C1q. Increased GFAP and C1q signals were observed in the *Unc119*$^{-/-}$ retina, suggesting activation of Müller glial cells in the *Unc119*$^{-/-}$ retina (Fig. 5B, 5C). One of the downregulated genes was nucleoredoxin-like 2 (*Nxnl2*), also known as rod-derived cone viability factor 2 (Rdcvf2). Rdcvf2 is a thioredoxin-like protein secreted by rods that promotes cone survival (Chalmel et al., 2007). We examined the expression levels of *Nxnl2* and *nucleoredoxin-like 1* (*Nxnl1*), which encodes Rdcvf, in *Unc119*$^{+/+}$ and *Unc119*$^{-/-}$ retinas using qRT-PCR analysis. We observed that the expression of *Nxnl2* and *Nxnl1* significantly decreased in *Unc119*$^{-/-}$ retinas compared to that in *Unc119*$^{+/+}$ retinas (Fig. 5D). Next, we performed gene set enrichment analysis (GSEA) (Wu et al., 2021) to identify differentially expressed gene modules between *Unc119*$^{+/+}$ and *Unc119*$^{-/-}$ mouse retinas (Fig. 5E). GSEA showed that genes related to immune responses were altered in the *Unc119*$^{-/-}$ mouse retina. Furthermore, we performed Ingenuity® Pathway Analysis (IPA) to predict upstream transcription factors affecting gene expression in the *Unc119*$^{-/-}$ retina. IPA predicted that *Irf1*, *Nfatc2*, *Ir3*, *Tp53*, *Nfkb1a*, *Rela*, *Irf7*, *Stat2*, *Stat3*, and *Klf6* were activated in the *Unc119*$^{-/-}$ retina (activation Z score > 3.0) (Fig. 5F). Almost all of the genes predicted to be activated are related to inflammation pathways, such as the JAK-STAT and NF-κB pathways. Notably, *Irf1*, a factor known to trigger the phosphorylation of STAT1 and thereby activate the JAK-STAT pathway (Guschin et al., 1995; Mishra and Ivashkiv, 2024), as well as *Rela*, a key member of the NF-κB protein family that governs NF-κB signaling (Ryseck et al., 1996), were activated. IPA networks showed that the transcription factors *Irf1* and *RelA* are upstream regulators of multiple inflammatory genes (Fig. 5G, 5H). These results suggest that *Unc119* deficiency directly or indirectly leads to activation of the JAK-STAT and NF-κB pathways, resulting in retinal inflammation.

Inhibition of the JAK-STAT and NF-κB pathways ameliorates cone degeneration by Unc119 deficiency

JNeurosci Accepted Manuscript

Based on the results of RNA-seq analysis and IPA, we hypothesized that suppression of the JAK-STAT and NF-κB pathways may ameliorate cone degeneration in the *Unc119*$^{-/-}$ mouse retina. We injected curcumin, an inhibitor of the JAK-STAT and NF-κB pathways (Ashrafizadeh et al., 2020; Wang et al., 2018), into *Unc119*$^{-/-}$ mice from P21 for seven days. At P28, we performed ERGs and histological analyses of control (DMSO-injected) *Unc119*$^{-/-}$ mice or curcumin-injected *Unc119*$^{-/-}$ mice (Fig. 6A). In the ERGs, we observed no significant differences in the amplitudes of scotopic a-, b-, and photopic a-waves. However, the amplitude of the photopic b-wave significantly increased in curcumin-treated mice, suggesting that curcumin partially rescued the decreased photopic b-wave amplitude observed in *Unc119*$^{-/-}$ mice at 1M (Fig. 6B, 6C, 6D, 6E, 6F, 6G). To examine whether curcumin suppresses the JAK-STAT and NF-κB pathways, we performed immunohistochemistry using an anti-Socs3 antibody for the JAK-STAT signature and an anti-RelA antibody for the NF-κB signature. Socs3 acts as a negative feedback regulator of the JAK-STAT pathway (Carow and Rottenberg, 2014, Hu et al., 2021), and RelA is one of the five NF-κB proteins (Liu et al., 2017). The signal intensities of Socs3 and RelA decreased in the curcumin-treated *Unc119*$^{-/-}$ retinas compared to those in the untreated *Unc119*$^{-/-}$ retinas, indicating that curcumin inhibits the JAK-STAT and NF-κB pathways (Fig. 6H, 6I). Next, we performed immunohistochemistry of the retinas of control and curcumin-injected *Unc119*$^{-/-}$ mice using anti-GFAP and anti-C1q antibodies. We measured the expression levels of GFAP and C1q in the retinas of the control and curcumin-injected mice to examine the effect of curcumin on inflammation. We observed a significant decrease in GFAP and C1q expression in the retinas of curcumin-treated mice, suggesting that curcumin suppressed inflammation resulting from *Unc119* deficiency (Fig. 6J, 6K). To assess the cone properties, we immunostained control and curcumin-injected *Unc119*$^{-/-}$ mouse retinas for M-opsin and S-opsin. The number of M-opsin and S-opsin signals was not significantly affected in the curcumin-injected mouse retinas. However, mislocalization of M-opsin and S-opsin signals in the OPL was observed in the retinal sections from control mice, but not significantly detected in those from curcumin-treated mice (Fig. 6L, 6M). These results suggest that curcumin can ameliorate cone degeneration resulted from *Unc119* deficiency by suppressing

JNeurosci Accepted Manuscript

inflammation in the retina through the downregulation of JAK-STAT and NF-κB pathway activities.

Inhibition of UNC119 binding to GNAT1or GNAT2 by UNC119-K57X CRD mutant

Finally, to investigate the pathological mechanisms underlying CRD associated with a human *UNC119* (hUNC119) mutation, we focused on a CRD mutation with a heterozygous A-to-T transition in codon 57, resulting in a lysine-to-premature termination codon (hUNC119-K57X) in the middle region of the hUNC119 protein (Kobayashi et al., 2000). We hypothesized that the hUNC119-K57X mutant would inhibit the interaction between hUNC119 and human GNAT1 (hGNAT1) or human GNAT2 (hGNAT2). To test this hypothesis, we performed immunoprecipitation analysis using plasmids expressing HA-tagged hUNC119, FLAG-tagged hGNAT1, FLAG-tagged hGNAT2, and Myc-tagged hUNC119-K57X. First, we examined the interaction between hUNC119 and hGNAT1 or hGNAT2 using immunoprecipitation and confirmed that hUNC119 interacts with both hGNAT1 and hGNAT2 (Fig. 7A). Next, we conducted an immunoprecipitation assay to determine whether the hUNC119-K57X mutant inhibited the interaction between hUNC119 and hGNAT1 or hGNAT2. The interaction between hUNC119 and hGNAT1 or hGNAT2 was inhibited in a dose-dependent manner by increasing the expression of the hUNC119-K57X mutant (Fig. 7B, 7C). We performed pull-down assays using GST and GST-fused hUNC119-K57X proteins with *Nrl*$^{+/+}$ and *Nrl*$^{-/-}$ retinal lysates, followed by western blotting for Gnat1, Gnat2, and Unc119. We did not observe an interaction between the hUNC119-K57X and Gnat1, Gnat2, or Unc119, suggesting that hUNC119-K57X indirectly inhibits the interaction between hUNC119 and hGNAT1 or hGNAT2 (Fig. S7). These results suggest that the hUNC119-K57X mutation competitively inhibits the functions of hGNAT1 and hGANT2, leading to the onset of CRD in a heterozygous hUNC119-K57X patient.

JNeurosci Accepted Manuscript

Discussion

In the current study, we observed retinal degeneration in *Unc119*$^{-/-}$ mice, resembling the pathology of CRD. Unc119 interacted with Gnat2 in cones, and Gnat2 localization was reduced in the *Unc119*$^{-/-}$ cone OS. RNA-seq results indicated a greater inflammatory state in *Unc119*$^{-/-}$ retinas. Curcumin administration suppressed inflammation and cone degeneration in *Unc119*$^{-/-}$ retinas. The hUNC119-K57X mutation associated with CRD inhibited the interaction between hUNC119 and hGNAT1 or hGNAT2, suggesting that the hUNC119-K57X mutation may competitively inhibit the function of hGNAT1 or hGNAT2. This study may advance our understanding of the pathological mechanisms underlying CRD and contribute to the development of novel therapeutic approaches.

Cone dysfunction followed by rod dysfunction in Unc119$^{-/-}$ *mice*

Electrophysiological and histological analyses of *Unc119*-deficient mice from 1M to 12M revealed pathological phenotypes similar to CRD (Fig. 2, 3, S3, S8). Cone dysfunction appeared at 1M, followed by progressive dysfunction and degeneration of cones and rods at 6M. Given that *Unc119* expression was enriched in photoreceptor cells, we focused our analysis on photoreceptor degeneration. We examined the ERGs b-wave implicit time and observed no significant differences between *Unc119*$^{+/+}$ and *Unc119*$^{-/-}$ mice at 1M, 6M, or 12M (Fig. 2G, 2H, 3G, 3H, S3G, S3H), suggesting that Unc119 does not play an essential role in synaptic transmission from photoreceptors to bipolar cells, while recent studies have reported that *Unc119* deletion reduces the steady-state glutamate release rate at rod synapses (Fehlhaber et al., 2023). Future studies on rod synapse in *Unc119*$^{-/-}$ mice might provide additional insights into a role of Unc119 in rod synapse architecture and function.

Unc119 interacts with Gnat2 in cones

JNeurosci Accepted Manuscript

Unc119 is known to interact with Gnat1 (Zhang et al., 2011) and the present study demonstrated that it also interacts with Gnat2 (Fig. 4C, 4D). Our pull-down and LC-MS/MS analysis results suggest that Ytdc2, Tba1a, and Hmmr also interact with Unc119 (Fig. 4B, 4C). Hmmr is a receptor for hyaluronic acid and plays an important role in cell migration, growth, and differentiation (Turley and Naor, 2012). In the eye, Hmmr is localized to the apical region of the retinal pigment epithelium and hyaluronan is a major component of the interphotoreceptor matrix (Hollyfield, 1999). Hmmr may be involved in photoreceptor survival. Examination of the possible functional interaction between Unc119 and Hmmr requires future analysis.

Additionally, in mice lacking the *Unc119* gene, we observed reduced Gnat2 signals in photoreceptor OS by immunohistochemistry; however, the total amount of Gnat2 protein in the retina remained unchanged (Fig. 4E, 4F, 4G). This result suggests that Gnat2 does not localize properly to the photoreceptor OS in *Unc119*-deficient mice, and that Unc119 may regulate Gnat2 transport in cones. It has been reported that a decrease in photopic ERGs responses without retinal degeneration occurs in adult mice lacking the *Gnat2* gene (Chang et al., 2006), suggesting that the reduced localization of Gnat2 in the OS may contribute to cone photoreceptor dysfunction in *Unc119*$^{-/-}$ retinas.

Unc119 and regulation of G protein α-subunit localization

The present study showed that Unc119 interacts with Gnat2 and is essential for its proper localization of Gnat2 in cones (Fig. 4E, 4F). Gnat1 is similarly regulated by Unc119 for its localization in rods (Zhang et al., 2011). In *C. elegans,* Unc119 regulates the proper localization of ODR-3 and GPA-13, G protein alpha subunits, in the cilia of olfactory sensory neurons (Zhang et al., 2011). Based on these findings, we speculate that Unc119 may interact with a G protein α-subunit and regulate its localization in cells other than retinal photoreceptor cells. For example, Gustducin and Gαolf, which are involved in taste and olfaction, respectively, are G protein α-subunits that possess glycine at the second amino acid residue in each protein. Further studies are needed to

JNeurosci Accepted Manuscript

examine whether Unc119 interacts with Gustducin and/or Gαolf in terms of taste and olfactory function. We observed no apparent changes in *Unc119*$^{-/-}$ mouse tissues except the retina as far as we examined. It should be noted that mouse Unc119 has a paralog, Unc119b, which might compensate for Unc119 function. Generating and analyzing *Unc119*$^{-/-}$*/Unc119b*$^{-/-}$ double-knockout mice may provide additional insights into the function of Unc119 in various tissues and cells.

Unc119 deficiency induces immune and inflammatory responses in the retina

Our RNA-seq analysis identified 80 downregulated and 286 upregulated genes in the *Unc119*$^{-/-}$ mouse retina compared to the control retina (Fig. 5A). Initially, we focused on GFAP as one of the upregulated genes. Although the expression level of GFAP is typically low in Müller glial cells, it is highly expressed in the retina with photoreceptor degeneration (Sarthy et al., 1991), suggesting that the increased expression of GFAP is linked to photoreceptor degeneration caused by *Unc119* deficiency. C1q, the first component of the classical complement pathway, is associated with pathological features of age-related neurodegenerative diseases such as amyloid-β accumulation in Alzheimer's disease, glaucomatous damage in glaucoma models, and drusen deposition in age-related macular degeneration (AMD) (Dejanovic et al., 2022; Howell et al., 2011; Greferath et al., 2024; Yednock et al., 2022). Furthermore, the classical complement pathway, mediated by C1q, has been shown to contribute to the progression of retinal degeneration (Jiao et al., 2018; Taylor et al., 2016). Thus, elevated C1q expression may play a role in retinal degeneration in *Unc119*$^{-/-}$ retinas. *Edn2* and *Fgf2*, genes commonly upregulated in retinal degeneration models (Rattner et al., 2008; Chen et al., 2004; Bramall et al., 2013; Samardzija et al., 2012; Kuny et al., 2012) were also upregulated in the *Unc119*$^{-/-}$ retina. Rdcvf2, an inactive thioredoxin secreted from rods, is equivalent to Rdcvf, which protects cones from degeneration (Chalmel et al., 2007). Thus, reduced expression of Rdcvf2 in the *Unc119*$^{-/-}$

JNeurosci Accepted Manuscript

retina may make cones more susceptible to degeneration. In addition, GSEA and IPA revealed elevated immune and inflammatory responses in *Unc119*$^{-/-}$ retinas (Fig. 5E, 5F). IPA further identified the activated transcription factors involved in the JAK-STAT and NF-κB signaling pathways in the *Unc119*$^{-/-}$ retina. This finding suggests that *Unc119* deficiency activates these pathways and promotes photoreceptor degeneration. Curcumin treatment downregulated GFAP and C1q expression and reduced the ectopic localization of M-opsin and S-opsin in *Unc119*$^{-/-}$ mouse retinas (Fig. 6), suggesting that curcumin treatment suppressed cone photoreceptor degeneration caused by *Unc119* deficiency. Overall, these results suggest that inhibition of the JAK-STAT and NF-κB signaling pathways ameliorates cone photoreceptor degeneration due to *Unc119* deficiency.

Pathogenesis of CRD with UNC119-K57X mutation

The present study elucidated a part of the pathological mechanism underlying CRD associated with a C-terminal region-defective hUNC119 mutant, in which the codon encoding the 57th amino acid becomes a termination codon (Kobayashi et al., 2000). The K57X mutation decreased the interaction between UNC119 and GNAT1 or GNAT2 in a dose-dependent manner in the immunoprecipitation assay (Fig. 7B, 7C). Mutations in the *GNAT1* gene have been reported to be associated with late-onset retinitis pigmentosa in humans (Carrigan et al., 2016). *Gnat1*-deficient mice show mild retinal degeneration with age (Calvert et al., 2000). *GNAT2* mutations are well known to cause color blindness in humans (Hassall et al., 2017). *Gnat2*-deficient mice exhibit decreased cone-mediated responses during adulthood (Chang et al., 2006). Our findings suggest that the hUNC119-K57X mutant competitively inhibits the interaction between UNC119 and GNAT1 or GNAT2, leading to partial loss of function of GNAT1 or GNAT2, which may result in retinal degeneration. We propose that UNC119-K57X-mediated disruption of the interaction between UNC119 and GNAT1 or GNAT2 contributes to CRD pathogenesis. Previous research has shown that transgenic mice overexpressing Unc119-K57X exhibited a reduced b-wave amplitude in ERGs and thinning of the

JNeurosci Accepted Manuscript

754 photoreceptor layer (Kobayashi et al., 2000). Further studies that generate and
755 analyze heterozygous Unc119-K57X knock-in mice may be useful to confirm
756 the pathological mechanism in vivo. Together, we propose a possible
757 mechanism of CRD associated with *UNC119* mutations, where the reduction in
758 UNC119 function leads to decreased activity of both GNAT1 and GNAT2,
759 accompanied by retinal inflammation, ultimately resulting in photoreceptor
760 degeneration (Fig. 7D).

JNeurosci Accepted Manuscript

Author Contributions

TC and TF designed the project. TC, RT, TT, and TF generated *Unc119*$^{-/-}$ mice. HY, TT and TF generated *Nrl*$^{-/-}$ mice. KK, TC, TH, YM, YN, and TF performed histological and molecular biological experiments. KK and YN carried out cell culture and biochemical experiments. KK, TC, and YM performed ERGs experiments. KK, TC and YM performed light-induced damage experiments. KK and DO performed RNA-seq experiments. KK, TC, and TF wrote the manuscript. TF supervised the project.

JNeurosci Accepted Manuscript

References

Ashrafizadeh M, Rafiei H, Mohammadinejad R, Afshar EG, Farkhondeh T, Samarghandian S (2020) Potential therapeutic effects of curcumin mediated by JAK/STAT signaling pathway: A review. Phytother Res 34:1745-1760.

Birtel J, Eisenberger T, Gliem M, Muller PL, Herrmann P, Betz C, Zahnleiter D, Neuhaus C, Lenzner S, Holz FG, Mangold E, Bolz HJ, Charbel Issa P (2018) Clinical and genetic characteristics of 251 consecutive patients with macular and cone/cone-rod dystrophy. Sci Rep 8:4824.

Bramall AN, Szego MJ, Pacione LR, Chang I, Diez E, D'Orleans-Juste P, Stewart DJ, Hauswirth WW, Yanagisawa M, McInnes RR (2013) Endothelin-2-mediated protection of mutant photoreceptors in inherited photoreceptor degeneration. PLoS One 8:e58023.

Brann MR, Cohen LV (1987) Diurnal expression of transducin mRNA and translocation of transducin in rods of rat retina. Science 235:585-587.

Calvert PD, Krasnoperova NV, Lyubarsky AL, Isayama T, Nicolo M, Kosaras B, Wong G, Gannon KS, Margolskee RF, Sidman RL, Pugh EN, Jr., Makino CL, Lem J (2000) Phototransduction in transgenic mice after targeted deletion of the rod transducin alpha -subunit. Proc Natl Acad Sci U S A 97:13913-13918.

Carow B, Rottenberg ME (2014) SOCS3, a Major Regulator of Infection and Inflammation. Front Immunol 5:58.

Carrigan M, Duignan E, Humphries P, Palfi A, Kenna PF, Farrar GJ (2016) A novel homozygous truncating GNAT1 mutation implicated in retinal degeneration. Br J Ophthalmol 100:495-500.

JNeurosci Accepted Manuscript

Chalmel F, Leveillard T, Jaillard C, Lardenois A, Berdugo N, Morel E, Koehl P, Lambrou G, Holmgren A, Sahel JA, Poch O (2007) Rod-derived Cone Viability Factor-2 is a novel bifunctional-thioredoxin-like protein with therapeutic potential. BMC Mol Biol 8:74.

Chang B, Dacey MS, Hawes NL, Hitchcock PF, Milam AH, Atmaca-Sonmez P, Nusinowitz S, Heckenlively JR (2006) Cone photoreceptor function loss-3, a novel mouse model of achromatopsia due to a mutation in Gnat2. Invest Ophthalmol Vis Sci 47:5017-5021.

Chaya T, Tsutsumi R, Varner LR, Maeda Y, Yoshida S, Furukawa T (2019) Cul3-Klhl18 ubiquitin ligase modulates rod transducin translocation during light-dark adaptation. EMBO J 38:e101409.

Chaya T, Ishikane H, Varner LR, Sugita Y, Maeda Y, Tsutsumi R, Motooka D, Okuzaki D, Furukawa T (2022) Deficiency of the neurodevelopmental disorder-associated gene Cyfip2 alters the retinal ganglion cell properties and visual acuity. Hum Mol Genet 31:535-547.

Chen L, Wu W, Dentchev T, Zeng Y, Wang J, Tsui I, Tobias JW, Bennett J, Baldwin D, Dunaief JL (2004) Light damage induced changes in mouse retinal gene expression. Exp Eye Res 79:239-247.

Cong L, Ran FA, Cox D, Lin S, Barretto R, Habib N, Hsu PD, Wu X, Jiang W, Marraffini LA, Zhang F (2013) Multiplex genome engineering using CRISPR/Cas systems. Science 339:819-823.

de Castro-Miro M, Tonda R, Escudero-Ferruz P, Andres R, Mayor-Lorenzo A, Castro J, Ciccioli M, Hidalgo DA, Rodriguez-Ezcurra JJ, Farrando J, Perez-Santonja JJ, Cormand B, Marfany G, Gonzalez-Duarte R (2016) Novel Candidate Genes and a Wide Spectrum of Structural and Point Mutations

JNeurosci Accepted Manuscript

Responsible for Inherited Retinal Dystrophies Revealed by Exome Sequencing. PLoS One 11:e0168966.

Dejanovic B et al. (2022) Complement C1q-dependent excitatory and inhibitory synapse elimination by astrocytes and microglia in Alzheimer's disease mouse models. Nat Aging 2:837-850.

Fehlhaber KE, Majumder A, Boyd KK, Griffis KG, Artemyev NO, Fain GL, Sampath AP (2023) A Novel Role for UNC119 as an Enhancer of Synaptic Transmission. Int J Mol Sci 24.

Gasparini SJ, Llonch S, Borsch O, Ader M (2019) Transplantation of photoreceptors into the degenerative retina: Current state and future perspectives. Prog Retin Eye Res 69:1-37.

Goc A, Angel TE, Jastrzebska B, Wang B, Wintrode PL, Palczewski K (2008) Different properties of the native and reconstituted heterotrimeric G protein transducin. Biochemistry 47:12409-12419.

Gorska MM, Stafford SJ, Cen O, Sur S, Alam R (2004) Unc119, a novel activator of Lck/Fyn, is essential for T cell activation. J Exp Med 199:369-379.

Greferath U, Fletcher E, Savige J, Mack HG (2024) Drusen and Other Retinal Findings in People With IgA Glomerulonephritis. Am J Ophthalmol 257:247-253.

Grossniklaus HE, Geisert EE, Nickerson JM (2015) Introduction to the Retina. Prog Mol Biol Transl Sci 134:383-396.

JNeurosci Accepted Manuscript

Guschin D, Rogers N, Briscoe J, Witthuhn B, Watling D, Horn F, Pellegrini S, Yasukawa K, Heinrich P, Stark GR, et al. (1995) A major role for the protein tyrosine kinase JAK1 in the JAK/STAT signal transduction pathway in response to interleukin-6. EMBO J 14:1421-1429.

Hamel CP (2007) Cone rod dystrophies. Orphanet J Rare Dis 2:7.

Hassall MM, Barnard AR, MacLaren RE (2017) Gene Therapy for Color Blindness. Yale J Biol Med 90:543-551.

Higashide T, McLaren MJ, Inana G (1998) Localization of HRG4, a photoreceptor protein homologous to Unc-119, in ribbon synapse. Invest Ophthalmol Vis Sci 39:690-698.

Higashide T, Murakami A, McLaren MJ, Inana G (1996) Cloning of the cDNA for a novel photoreceptor protein. J Biol Chem 271:1797-1804.

Hollyfield JG (1999) Hyaluronan and the functional organization of the interphotoreceptor matrix. Invest Ophthalmol Vis Sci 40:2767-2769.

Howell GR, Macalinao DG, Sousa GL, Walden M, Soto I, Kneeland SC, Barbay JM, King BL, Marchant JK, Hibbs M, Stevens B, Barres BA, Clark AF, Libby RT, John SW (2011) Molecular clustering identifies complement and endothelin induction as early events in a mouse model of glaucoma. J Clin Invest 121:1429-1444.

Hu X, Li J, Fu M, Zhao X, Wang W (2021) The JAK/STAT signaling pathway: from bench to clinic. Signal Transduct Target Ther 6:402.

JNeurosci Accepted Manuscript

887 Huang L, Li S, Xiao X, Jia X, Wang P, Guo X, Zhang Q (2013) Screening for
888 variants in 20 genes in 130 unrelated patients with cone-rod dystrophy. Mol
889 Med Rep 7:1779-1785.

890

891 Ishiba Y, Higashide T, Mori N, Kobayashi A, Kubota S, McLaren MJ, Satoh H,
892 Wong F, Inana G (2007) Targeted inactivation of synaptic HRG4 (UNC119)
893 causes dysfunction in the distal photoreceptor and slow retinal degeneration,
894 revealing a new function. Exp Eye Res 84:473-485.

895

896 Jiao H, Rutar M, Fernando N, Yednock T, Sankaranarayanan S, Aggio-Bruce R,
897 Provis J, Natoli R (2018) Subretinal macrophages produce classical
898 complement activator C1q leading to the progression of focal retinal
899 degeneration. Mol Neurodegener 13:45.

900

901 Kerov V, Rubin WW, Natochin M, Melling NA, Burns ME, Artemyev NO (2007)
902 N-terminal fatty acylation of transducin profoundly influences its localization and
903 the kinetics of photoresponse in rods. J Neurosci 27:10270-10277.

904

905 Kobayashi A, Higashide T, Hamasaki D, Kubota S, Sakuma H, An W, Fujimaki
906 T, McLaren MJ, Weleber RG, Inana G (2000) HRG4 (UNC119) mutation found
907 in cone-rod dystrophy causes retinal degeneration in a transgenic model. Invest
908 Ophthalmol Vis Sci 41:3268-3277.

909

910 Koike C, Nishida A, Ueno S, Saito H, Sanuki R, Sato S, Furukawa A, Aizawa S,
911 Matsuo I, Suzuki N, Kondo M, Furukawa T (2007) Functional roles of Otx2
912 transcription factor in postnatal mouse retinal development. Mol Cell Biol
913 27:8318-8329.

914

915 Kozuka T, Chaya T, Tamalu F, Shimada M, Fujimaki-Aoba K, Kuwahara R,
916 Watanabe SI, Furukawa T (2017) The TRPM1 Channel Is Required for

JNeurosci Accepted Manuscript

917 Development of the Rod ON Bipolar Cell-AII Amacrine Cell Pathway in the
918 Retinal Circuit. J Neurosci 37:9889-9900.

919

920 Kuny S, Gaillard F, Sauve Y (2012) Differential gene expression in eyecup and
921 retina of a mouse model of Stargardt-like macular dystrophy (STGD3). Invest
922 Ophthalmol Vis Sci 53:664-675.

923

924 Liu T, Zhang L, Joo D, Sun SC (2017) NF-kappaB signaling in inflammation.
925 Signal Transduct Target Ther 2:17023-.

926

927 Lobanova ES, Herrmann R, Finkelstein S, Reidel B, Skiba NP, Deng WT, Jo R,
928 Weiss ER, Hauswirth WW, Arshavsky VY (2010) Mechanistic basis for the
929 failure of cone transducin to translocate: why cones are never blinded by light. J
930 Neurosci 30:6815-6824.

931

932 Maduro M, Pilgrim D (1995) Identification and cloning of unc-119, a gene
933 expressed in the Caenorhabditis elegans nervous system. Genetics 141:977-
934 988.

935

936 Mears AJ, Kondo M, Swain PK, Takada Y, Bush RA, Saunders TL, Sieving PA,
937 Swaroop A (2001) Nrl is required for rod photoreceptor development. Nat Genet
938 29:447-452.

939

940 Mishra B, Ivashkiv LB (2024) Interferons and epigenetic mechanisms in training,
941 priming and tolerance of monocytes and hematopoietic progenitors. Immunol
942 Rev 323:257-275.

943

944 Palko SI, Saba NJ, Mullane E, Nicholas BD, Nagasaka Y, Ambati J, Gelfand
945 BD, Ishigami A, Bargagna-Mohan P, Mohan R (2022) Compartmentalized

JNeurosci Accepted Manuscript

946 citrullination in Muller glial endfeet during retinal degeneration. Proc Natl Acad
947 Sci U S A 119.

948

949 Philp NJ, Chang W, Long K (1987) Light-stimulated protein movement in rod
950 photoreceptor cells of the rat retina. FEBS Lett 225:127-132.

951

952 Rattner A, Toulabi L, Williams J, Yu H, Nathans J (2008) The genomic response
953 of the retinal pigment epithelium to light damage and retinal detachment. J
954 Neurosci 28:9880-9889.

955

956 Ryseck RP, Weih F, Carrasco D, Bravo R (1996) RelB, a member of the
957 Rel/NF-kappa B family of transcription factors. Braz J Med Biol Res 29:895-903.

958

959 Samardzija M, Wariwoda H, Imsand C, Huber P, Heynen SR, Gubler A, Grimm
960 C (2012) Activation of survival pathways in the degenerating retina of rd10
961 mice. Exp Eye Res 99:17-26.

962

963 Sarthy PV, Fu M, Huang J (1991) Developmental expression of the glial fibrillary
964 acidic protein (GFAP) gene in the mouse retina. Cell Mol Neurobiol 11:623-637.

965

966 Sugita Y, Yamamoto H, Maeda Y, Furukawa T (2020) Influence of Aging on the
967 Retina and Visual Motion Processing for Optokinetic Responses in Mice. Front
968 Neurosci 14:586013.

969

970 Swanson DA, Chang JT, Campochiaro PA, Zack DJ, Valle D (1998) Mammalian
971 orthologs of C. elegans unc-119 highly expressed in photoreceptors. Invest
972 Ophthalmol Vis Sci 39:2085-2094.

973

JNeurosci Accepted Manuscript

Swaroop A, Xu JZ, Pawar H, Jackson A, Skolnick C, Agarwal N (1992) A conserved retina-specific gene encodes a basic motif/leucine zipper domain. Proc Natl Acad Sci U S A 89:266-270.

Taylor L, Arner K, Blom AM, Ghosh F (2016) Complimentary action: C1q increases ganglion cell survival in an in vitro model of retinal degeneration. J Neuroimmunol 298:117-129.

Tsang SH, Sharma T (2018) Progressive Cone Dystrophy and Cone-Rod Dystrophy (XL, AD, and AR). Adv Exp Med Biol 1085:53-60.

Tsutsumi R, Chaya T, Furukawa T (2018) Enriched expression of the ciliopathy gene Ick in cell proliferating regions of adult mice. Gene Expr Patterns 29:18-23.

Tsutsumi R, Chaya T, Tsujii T, Furukawa T (2022) The carboxyl-terminal region of SDCCAG8 comprises a functional module essential for cilia formation as well as organ development and homeostasis. J Biol Chem 298:101686.

Turley EA, Naor D (2012) RHAMM and CD44 peptides-analytic tools and potential drugs. Front Biosci (Landmark Ed) 17:1775-1794.

Varner LR, Chaya T, Maeda Y, Tsutsumi R, Zhou S, Tsujii T, Okuzaki D, Furukawa T (2024) The deubiquitinase Otud7b suppresses cone photoreceptor degeneration in mouse models of retinal degenerative diseases. iScience 27:109380.

Vepachedu R, Karim Z, Patel O, Goplen N, Alam R (2009) Unc119 protects from Shigella infection by inhibiting the Abl family kinases. PLoS One 4:e5211.

JNeurosci Accepted Manuscript

Wang Y, Tang Q, Duan P, Yang L (2018) Curcumin as a therapeutic agent for blocking NF-kappaB activation in ulcerative colitis. Immunopharmacol Immunotoxicol 40:476-482.

Watanabe S, Sanuki R, Sugita Y, Imai W, Yamazaki R, Kozuka T, Ohsuga M, Furukawa T (2015) Prdm13 regulates subtype specification of retinal amacrine interneurons and modulates visual sensitivity. J Neurosci 35:8004-8020.

Wenzel A, Reme CE, Williams TP, Hafezi F, Grimm C (2001) The Rpe65 Leu450Met variation increases retinal resistance against light-induced degeneration by slowing rhodopsin regeneration. J Neurosci 21:53-58.

Whelan JP, McGinnis JF (1988) Light-dependent subcellular movement of photoreceptor proteins. J Neurosci Res 20:263-270.

Wu T, Hu E, Xu S, Chen M, Guo P, Dai Z, Feng T, Zhou L, Tang W, Zhan L, Fu X, Liu S, Bo X, Yu G (2021) clusterProfiler 4.0: A universal enrichment tool for interpreting omics data. Innovation (Camb) 2:100141.

Yamamoto H, Kon T, Omori Y, Furukawa T (2020) Functional and Evolutionary Diversification of Otx2 and Crx in Vertebrate Retinal Photoreceptor and Bipolar Cell Development. Cell Rep 30:658-671 e655.

Yednock T, Fong DS, Lad EM (2022) C1q and the classical complement cascade in geographic atrophy secondary to age-related macular degeneration. Int J Retina Vitreous 8:79.

JNeurosci Accepted Manuscript

Yoshimoto T, Chaya T, Varner LR, Ando M, Tsujii T, Motooka D, Kimura K, Furukawa T (2023) The Rax homeoprotein in Muller glial cells is required for homeostasis maintenance of the postnatal mouse retina. J Biol Chem 299:105461.

Zenteno JC, Arce-Gonzalez R, Matsui R, Lopez-Bolanos A, Montes L, Martinez-Aguilar A, Chacon-Camacho OF (2023) Clinical-genetic findings in a group of subjects with macular dystrophies due to mutations in rare inherited retinopathy genes. Graefes Arch Clin Exp Ophthalmol 261:353-365.

Zhang H, Constantine R, Vorobiev S, Chen Y, Seetharaman J, Huang YJ, Xiao R, Montelione GT, Gerstner CD, Davis MW, Inana G, Whitby FG, Jorgensen EM, Hill CP, Tong L, Baehr W (2011) UNC119 is required for G protein trafficking in sensory neurons. Nat Neurosci 14:874-880.

JNeurosci Accepted Manuscript

Figure Legends

Figure 1. Generation of *Unc119*$^{-/-}$ mice

A. RT-PCR analysis of *Unc119* transcripts in mouse tissues at 4 wks.

B. *In situ* hybridization analysis of *Unc119* transcripts in developing E17.5, P3, P9, and P14 retinas. GCL, ganglion cell layer; NBL, neuroblastic layer; ONL, outer nuclear layer; INL, inner nuclear layer.

C. DNA sequences of exon 1 in wild-type and *Unc119* mutant mice. Seven, one, and fifty-seven base-pair (bp) deletions (total 65 bp deletion) resulted in a transcriptional frameshift and premature stop codon.

D. Schematic representation of the *Unc119* mutant allele.

E. PCR products of 195 bp and 260 bp were amplified from the wild-type and *Unc119* mutant alleles, respectively.

F. RT-PCR analysis of *Unc119* transcripts in *Unc119*$^{+/+}$ and *Unc119*$^{-/-}$ retinas. β-Actin was used as a loading control.

G. Western blot analysis of Unc119 protein in *Unc119*$^{+/+}$ and *Unc119*$^{-/-}$ mouse retinas. α-tubluin was used as a loading control.

H. Immunofluorescence analysis of Unc119 protein in *Unc119*$^{+/+}$ and *Unc119*$^{-/-}$ mouse retinas.

I, J. Subcellular localization of Gnat1 in photoreceptor cells of *Unc119*$^{+/+}$ and *Unc119*$^{-/-}$ retinas under dark- and light-adapted conditions at 1M. The measured Gnat1 signals in the ONL of the photoreceptors are shown. Data are presented as the mean ± SD. n = 3 mice. ***P < 0.001, n.s., not significant (unpaired t-test). GCL, ganglion cell layer; ONL, outer nuclear layer; INL, inner nuclear layer; OS, outer segment.

Figure 2. Decreased cone light responses in *Unc119*$^{-/-}$ mice at 1 M

JNeurosci Accepted Manuscript

A-F. ERGs analysis of *Unc119*$^{-/-}$ mice. ERGs were recorded from *Unc119*$^{+/+}$ and *Unc119*$^{-/-}$ mice at 1 M (n = 5 per each genotype). (***A***) Representative scotopic ERGs elicited by four stimulus intensities (-4.0 to 1.0 log cd s/m^2) from *Unc119*$^{+/+}$ and *Unc119*$^{-/-}$ mice at 1 M. (***B, C***) Scotopic amplitudes of a- (***B***) and b-waves (***C***) are shown as a function of stimulus intensity. Data are presented as the mean ± SD. n = 5 per each genotype. n.s., not significant (two-way repeated measures ANOVA, multiple comparisons). (***D***) Representative photopic ERGs elicited by four stimulus intensities (-0.5 to 1.0 log cd s/m^2) from *Unc119*$^{+/+}$ and *Unc119*$^{-/-}$ mice at 1 M. (***E, F***) Photopic amplitudes of a- (***E***) and b-waves (***F***) are shown as a function of the stimulus intensity. Data are presented as the mean ± SD. n = 5 per each genotype. *P < 0.05, ***P < 0.001, n.s., not significant (two-way repeated measures ANOVA, multiple comparison).

G, H. Scotopic and photopic b-wave implicit times of ERGs were recorded from *Unc119*$^{+/+}$ and *Unc119*$^{-/-}$ mice at 1M. The scotopic implicit times of the b-wave (***G***) reflect synaptic transmission from rod photoreceptors to rod bipolar rod cells. The photopic implicit times of the b-wave (***H***) reflect synaptic transmission from the cone photoreceptor to the cone ON bipolar cells. Data are presented as mean ± SD. n = 5 per each genotype. n.s., not significant (two-way repeated measures ANOVA, multiple comparison).

I. Toluidine blue staining of *Unc119*$^{+/+}$ and *Unc119*$^{-/-}$ retinas at 1M. The thicknesses of the ONL, OPL, INL, IPL, and GCL were measured using ImageJ. Data are presented as the mean ± SD. n = 4 per each genotype. n.s., not significant (unpaired t-test). GCL, ganglion cell layer; ONL, outer nuclear layer; INL, inner nuclear layer; IPL, inner plexiform layer.

J-R. Immunofluorescence analysis of retinal sections from *Unc119*$^{+/+}$ and *Unc119*$^{-/-}$ at 1M using marker antibodies as follows: Rhodopsin (rod outer segments, ***J***), M-opsin (M-cone outer segments, ***K***), S-opsin (S-cone outer segments, ***L***), Chx10 (bipolar cells, ***M***), Pax6 (amacrine and ganglion cells, ***N***), Calbindin (horizontal cells and a subset of amacrine cells, ***O***), Ctbp2 (photoreceptor synapses, ***P***), Rbpms (ganglion cells, ***Q***), and S100β (Müller glial cells, ***R***). The nuclei were stained with DAPI (blue). Rhodopsin length was measured in four images from the retina of one mouse. In one image,

JNeurosci Accepted Manuscript

Rhodopsin length was measured at three points and averaged (***J***). The signal intensity of M-opsin and S-opsin in OPL were measured. Arrowheads indicate mislocalization of M-opsin and S-opsin signals (***K, L***). Data are presented as the mean ± SD. n = 3 per each genotype. n.s., not significant (unpaired t-test). GCL, ganglion cell layer; ONL, outer nuclear layer; INL, inner nuclear layer; OS, outer segment.

Figure 3. Decrease in cone and rod light responses of *Unc119*$^{-/-}$ mice at 12M

A-F. ERGs analysis of *Unc119*$^{-/-}$ mice at 12M. ERGs were recorded from *Unc119*$^{+/+}$ and *Unc119*$^{-/-}$ mice at 12M (n = 5 and 4 mice, *Unc119*$^{+/+}$ and *Unc119*$^{-/-}$, respectively). (***A***) Representative scotopic ERGs elicited by four stimulus intensities (-4.0 to 1.0 log cd s/m^2) from *Unc119*$^{+/+}$ and *Unc119*$^{-/-}$ mice at 12M. (***B, C***) The scotopic amplitudes of a- (***B***) and b-waves (***C***) are shown as a function of the stimulus intensity. Data are presented as the mean ± SD. n = 5 and 4 mice (*Unc119*$^{+/+}$ and *Unc119*$^{-/-}$ mice, respectively). **P < 0.01, ***P < 0.001, n.s., not significant (two-way repeated measures ANOVA, multiple comparison). (***D***) Representative photopic ERGs elicited by four stimulus intensities (-0.5 to 1.0 log cd s/m^2) from *Unc119*$^{+/+}$ and *Unc119*$^{-/-}$ mice at 12M. (***E, F***) The photopic amplitudes of a- (***E***) and b-waves (***F***) are shown as a function of the stimulus intensity. Data are presented as mean ± SD. n = 5 and 4 mice (*Unc119*$^{+/+}$ and *Unc119*$^{-/-}$, respectively). *P < 0.05, **P < 0.01, n.s., not significant (two-way repeated measures ANOVA, multiple comparison).

G, H. Scotopic (***G***) and photopic (***H***) b-wave implicit times of ERGs were recorded from *Unc119*$^{+/+}$ and *Unc119*$^{-/-}$ mice at 12M. Data are presented as the mean ± SD. n = 5 and n = 4 mice, *Unc119*$^{+/+}$ and *Unc119*$^{-/-}$, respectively. n.s., not significant (two-way repeated measures ANOVA, multiple comparisons).

I. Toluidine blue staining of *Unc119*$^{+/+}$ and *Unc119*$^{-/-}$ retinas at 12 M. The thicknesses of the ONL, OPL, INL, IPL, and GCL were measured using ImageJ. Data are presented as the mean ± SD. n = 3 and 4 (*Unc119*$^{+/+}$ and *Unc119*$^{-/-}$, respectively). *P < 0.05, ***P < 0.01, ****P<0.001, n.s., not significant (unpaired

JNeurosci Accepted Manuscript

t-test (upper bar graph) and one-way ANOVA, multiple comparisons (lower bar graph)). GCL, ganglion cell layer; ONL, outer nuclear layer; INL, inner nuclear layer; IPL, inner plexiform layer; OS, outer segment.

J-M. Immunofluorescence analysis of retinal sections from *Unc119*$^{+/+}$ and *Unc119*$^{-/-}$ at 12M using marker antibodies as follows: Rhodopsin (rod outer segments, ***J***), M-opsin (M-cone outer segments, ***K***), S-opsin (S-cone outer segments, ***L***), and Arr3 (cone photoreceptor cells, ***M***). Nuclei were stained with DAPI (blue). Rhodopsin length was measured in four images from the retina of one mouse. In one image, Rhodopsin length was measured at three points and averaged (***J***). The number of M-opsin-, S-opsin-, and Arr3-positive cells was counted (***K, L, M***). Data are presented as mean ± SD. n = 3 and 4 (*Unc119*$^{+/+}$ and *Unc119*$^{-/-}$, respectively). *P < 0.05, **P < 0.01, ***P < 0.001 (unpaired t-test). GCL, ganglion cell layer; ONL, outer nuclear layer; INL, inner nuclear layer; OS, outer segment.

Figure 4. Unc119 interacts with Gnat2 in cones

A. Generation of *Nrl*$^{-/-}$ mice and western blotting analysis of *Nrl*$^{+/+}$ and *Nrl*$^{-/-}$ mouse retinas using the following antibodies: Rhodopsin, S-opsin, and M-opsin. α-Tubulin was used as a loading control.

B. Scheme of pull-down assay and LC-MS/MS analysis. A pull-down assay was performed using GST and GST-fused Unc119 proteins. GST- and GST-fused Unc119 proteins were reacted with *Nrl*$^{-/-}$ retinal lysates or lysis buffer. Venn diagram of the number of identified proteins in the indicated experimental conditions by pull-down assay and subsequent LC-MS/MS analysis (left).
C. Fifty-eight proteins were identified using total LC-MS/MS analysis. Four proteins, Gnat2, Ytdc2, Tba1a, and Hmmr, were detected only in GST-fused mUnc119 that reacted with *Nrl*$^{-/-}$ retinal lysates. The normalized total spectra of Gnat2 are shown.
D. Immunoprecipitation of Unc119 with Gnat1 or Gnat2. Plasmids expressing FLAG-tagged Gnat1 or Gnat2, and HA-tagged Unc119 were co-transfected into

JNeurosci Accepted Manuscript

HEK293T cells. Cell lysates were subjected to immunoprecipitation using an anti-FLAG antibody. The immunoprecipitated proteins were detected by western blot analysis using anti-FLAG and anti-HA antibodies.

E,F. Immunofluorescence analysis of *Unc119*$^{+/+}$ and *Unc119*$^{-/-}$ retinas at 1M (***D***) and P14 (***E***), using an anti-Gnat2 antibody. Nuclei were stained with DAPI (blue). Gnat2 intensity was measured in the retinal sections of all photoreceptor layers (OS, IS, ONL, and OPL) using ImageJ software. Data are presented as the mean ± SD. n = 5 per each genotype at 1 M and n = 3 per each genotype at P14. ***P < 0.001, (unpaired t-test). GCL, ganglion cell layer; ONL, outer nuclear layer; INL, inner nuclear layer; OS, outer segment.

G. Western blotting analysis of Gnat2 protein in retinas from *Unc119*$^{+/+}$ and *Unc119*$^{-/-}$ mice at P14 using an anti-Gnat2 antibody. α-Tubulin was used as a loading control. Relative Gnat2 protein levels in *Unc119*$^{+/+}$ and *Unc119*$^{-/-}$ retinas were determined by quantification of Gnat2 band intensity (normalized to α-tubulin). Data are presented as the mean ± SD. n.s., not significant (unpaired t-test); n = 5 mice per genotype.

H, I. Immunoprecipitation analysis of Unc119 and Gnat1, Gnat1-G2A, Gnat2, or Gnat2-G2A. Plasmids expressing FLAG-tagged Gnat1, Gnat1-G2A, Gnat2, or Gnat2-G2A, and HA-tagged Unc119 were co-transfected into HEK293T cells. Cell lysates were subjected to immunoprecipitation with an anti-FLAG antibody. Immunoprecipitated proteins were detected by Western blot analysis with anti-FLAG (***H***) and anti-HA (***I***) antibodies.

Figure 5. Transcriptional changes by *Unc119* deficiency in the retina

A. Heatmaps of differentially expressed genes (fold change > 1.4, <-1.4; p < 0.05, unpaired t-test) between *Unc119*$^{+/+}$ and *Unc119*$^{-/-}$ retinas. Normalized FPKM from the RNA-seq dataset was used for heatmap visualization.

B, C. Immunofluorescence analysis of *Unc119*$^{+/+}$ and *Unc119*$^{-/-}$ retinas at 1M using antibodies against GFAP and C1q. Nuclei were stained with DAPI (blue).

JNeurosci Accepted Manuscript

The intensities of GFAP (***B***) and C1q (***C***) signals in *Unc119*$^{+/+}$ and *Unc119*$^{-/-}$ retinas at 1M were measured. Data are presented as the mean ± SD. ∗∗p < 0.01 (unpaired t-test). n = 3 mice per group. GCL, ganglion cell layer; ONL, outer nuclear layer; INL, inner nuclear layer

D. qRT-PCR analysis of *Nxnl2* and *Nxnl1* mRNA expression levels in the *Unc119*$^{+/+}$ and *Unc119*$^{-/-}$ mouse retinas. Data are presented as the mean ± SD. ∗p < 0.05, ∗∗p < 0.01 (unpaired t-test). n = 3 mice per group.

E. Gene set enrichment analysis of upregulated genes in the *Unc119*$^{-/-}$ mouse retina.

F. Ingenuity® Pathway Analysis (IPA) to predict the upstream factors affecting gene expression changes (fold change > 1.4, <-1.4; p < 0.05, unpaired t-test) in the *Unc119*$^{-/-}$ retina. The predicted upstream factors with an activation Z score > 3.0, are shown.

G, H. IPA networks showing interferon regulatory factor 1 (IRF1) (***G***) and RELA proto-Oncogene (***H***), NF-kB subunit (RELA) as upstream regulators. IRF1 and RELA were predicted to be activated in the *Unc119*$^{-/-}$ mouse retina.

Figure 6. Curcumin suppresses cone degeneration and inflammation in the *Unc119*$^{-/-}$ retina

A. Experimental design for curcumin administration to *Unc119*$^{-/-}$ mice.

B-G. ERGs analysis of curcumin-treated *Unc119*$^{-/-}$ mice at 1M. ERGs were recorded from control (DMSO) and curcumin-treated *Unc119*$^{-/-}$ mice at 1M (n = 4 per each genotype). (***B***) Representative scotopic ERGs elicited by four stimulus intensities (-4.0 to 1.0 log cd s/m2) from control (DMSO) and curcumin-treated *Unc119*$^{-/-}$ mice at 1M. (***C, D***) The scotopic amplitudes of a- (***C***) and b-waves (***D***) are shown as a function of the stimulus intensity. Data are presented as the mean ± SD. n = 4 per each genotype. n.s., not significant (two-way

JNeurosci Accepted Manuscript

repeated measures ANOVA, multiple comparisons). (***E***) Representative photopic ERGs elicited by four stimulus intensities (-0.5 to 1.0 log cd s/m2) from control (DMSO) and curcumin-treated Unc119$^{-/-}$ mice at 1M. (***F, G***) Photopic amplitudes of a- (***F***) and b-waves (***G***) are shown as functions of stimulus intensity. Data are presented as the mean ± SD. n = 4 mice per each genotype. *P < 0.05, n.s., not significant (two-way repeated measures ANOVA, multiple comparison).

H-M. Immunofluorescence analysis of retinal sections from control and curcumin-injected *Unc119*$^{-/-}$ mice was performed using antibodies against Socs3 (***H***), RelA (***I***), GFAP (***J***), C1q (***K***), M-opsin (***L***), and S-opsin (***M***). Nuclei were stained with DAPI (blue). The intensities of the Socs3, RelA, GFAP and C1q signals in the retina were measured (***H, I, J, K***). The number of M-opsin- and S-opsin-positive cells was counted. The signal intensities of M-opsin and S-opsin in the OPL were measured. Arrowheads indicate mislocalization of M-opsin and S-opsin signals (***L, M***). Data are presented as mean ± SD. n = 4 per each genotype. *P < 0.05, **P < 0.01, ***P < 0.001, n.s., not significant (unpaired t-test). GCL, ganglion cell layer; ONL, outer nuclear layer; INL, inner nuclear layer; OS, outer segment.

Figure 7. Inhibition of UNC119 interaction with GNAT1 or GNAT2 by UNC119-K57X

A. Immunoprecipitation analysis of human UNC119 (hUNC119) with hGNAT1 or hGNAT2. Plasmids expressing FLAG-tagged hGNAT1 or hGNAT2, and HA-tagged hUNC119 were co-transfected into HEK293T cells. The cell lysates were subjected to immunoprecipitation with the anti-FLAG antibody. Immunoprecipitated proteins were detected by Western blot analysis with anti-FLAG and anti-HA antibodies.

B, C. Myc-tagged hUNC119-K57X, in addition to the expression constructs used in A, were co-transfected into HEK293T cells. The cell lysates were subjected to immunoprecipitation with the anti-FLAG antibody. Immunoprecipitated proteins were detected by Western blot analysis with anti-FLAG and anti-HA antibodies. Relative intensities were determined by

JNeurosci Accepted Manuscript

quantification of IP: HA band intensities (normalized to Input: HA) using ImageJ software.

D*.* A hypothetical model of CRD caused by compromised Unc119 function.

JNeurosci Accepted Manuscript

1259 **Table 1 Primer sequence**

Primer name	Sequence (5'→3')
mUnc119-RT-PCR-51	TCCTTTTTGAAATCAAGAAGCCCCCTG
mUnc119-RT-PCR-31	TTTCGAAAGTAGTGCCTCTCGATCATG
mUnc119-RT-PCR-52	GAGGGCAAGCAGCCCATCGGGCCGGAG
mUnc119-RT-PCR-32	GGTCCAGGTCCCGCCGGTTGATGGGCA
mGnat1-kozak-ORF-EcoRI-51	GAATTCGCCACCATGGGGGCTGGGGCCAGCGCTGAGGAG
mGnat1-ORF-NotI-31	GCGGCCGCAGAAGAGCCCGCAGTCTTTGAGGTTCTC
mGnat2-ORF-kozak-XhoI-51	TCTCGAGCCACCATGGGGAGTGGCATCAGTGCTGAGGAC
mGnat2-ORF-wostop-NotI-31	TGCGGCCGCAAAAGAGCCCACAGTCCTTGAGGTTTTC
mGnat1-kozak-ORF-G2A-EcoRI-51	GAATTCGCCACCATGGCCGCTGGGGCCAGCGCTGAGGAG
mGnat2-ORF-kozak-G2A-XhoI-51	TCTCGAGCCACCATGGCCAGTGGCATCAGTGCTGAGGAC
mNxnl2-qPCR-51	GACTTCTACACGGAGCTGGTGAGCGAG
mNxnl2-qPCR-31	TTGGGGATGGCGGTGATTTCGTACCTC
mNxnl1-qPCR-51	ACTGACCAGTTCTACGTGCTGCGGGCA
mNxnl1-qPCR-31	ACAACCGCTGGCAGTTGACGGACAGAG
hGNAT1-ORF-kozak-SalI-51	GGGGTCGACGCCACCATGGGGGCTGGGGCCAGTGCTG

JNeurosci Accepted Manuscript

hGNAT1-ORF-NotI-31	GGGGCGGCCGCAGAAGAGGCCACAGTCTTTGAGGTTC
hGNAT2-ORF-kozak-XhoI-51	GGGCTCGAGCCACCATGGGAAGTGGAGCCAGTGCTGAGGACA
hGNAT2-ORF-NotI-31	GGGGCGGCCGCAGAAGAGGCCGCAGTCCTTGAGGTTTTC
hUNC119-ORF-XhoI-53	GGGCTCGAGATGAAGGTGAAGAAGGGCGGCGGT
hUNC119-ORF-NotI-34	GGGGCGGCCGCTCAGGGTGTCCCGCTGTAGGA
hUNC119-K57X-NotI-31	GGGGCGGCCGCCTACCTCTGCAGCGGCCCCGGCCTG

gRNA	Sequence (5'→3')
mUnc119-gRNA1	AGGGGCCTCGAACCGGAGCGCGG
mUnc119-gRNA2	AGCACATCCTCCGGCCCGATGGG
mNrl-gRNA	GCTGAGTCCCGACGAAGCTGTGG

JNeurosci Accepted Manuscript

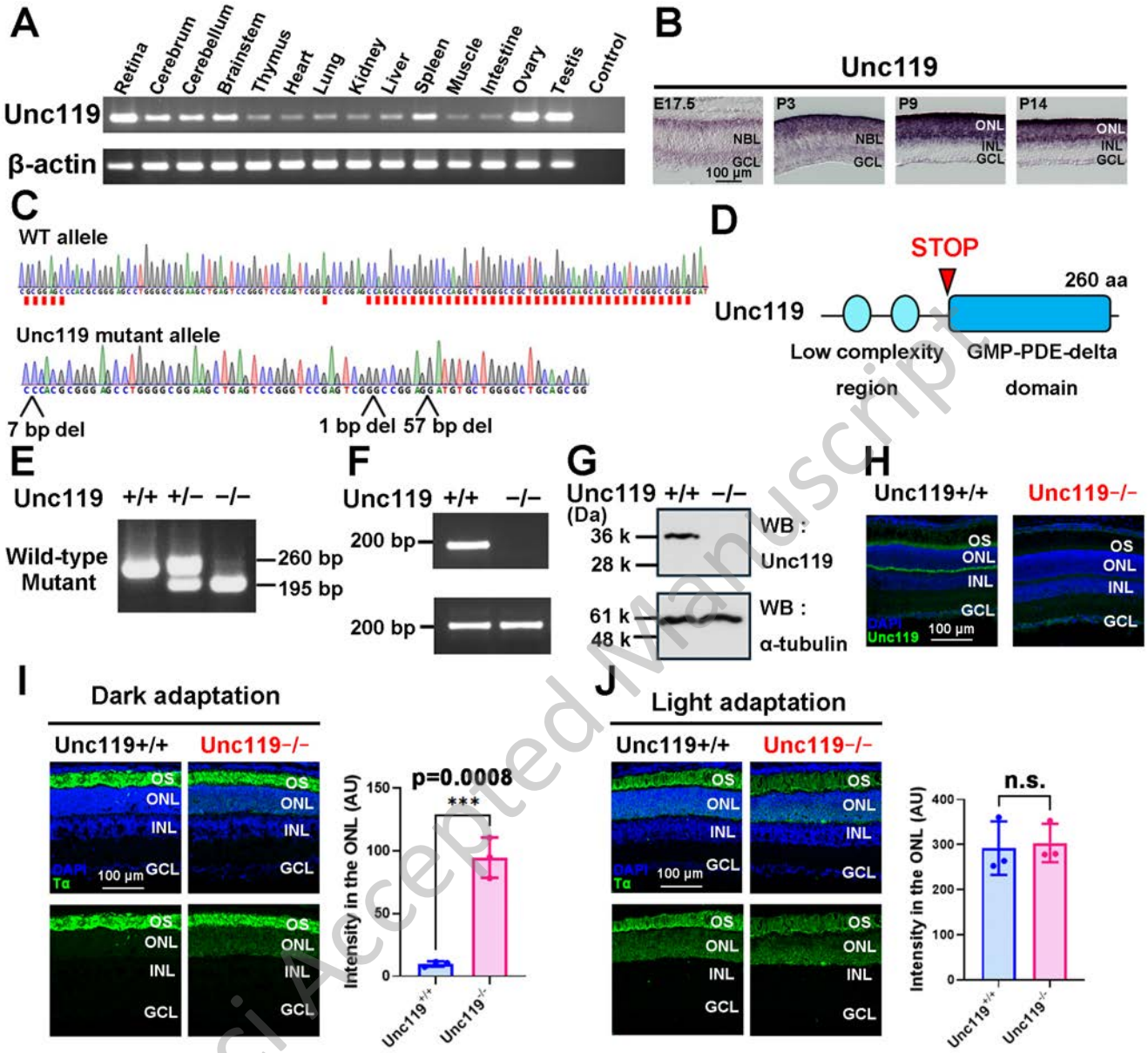

Figure 1

JNeurosci Accepted Manuscript

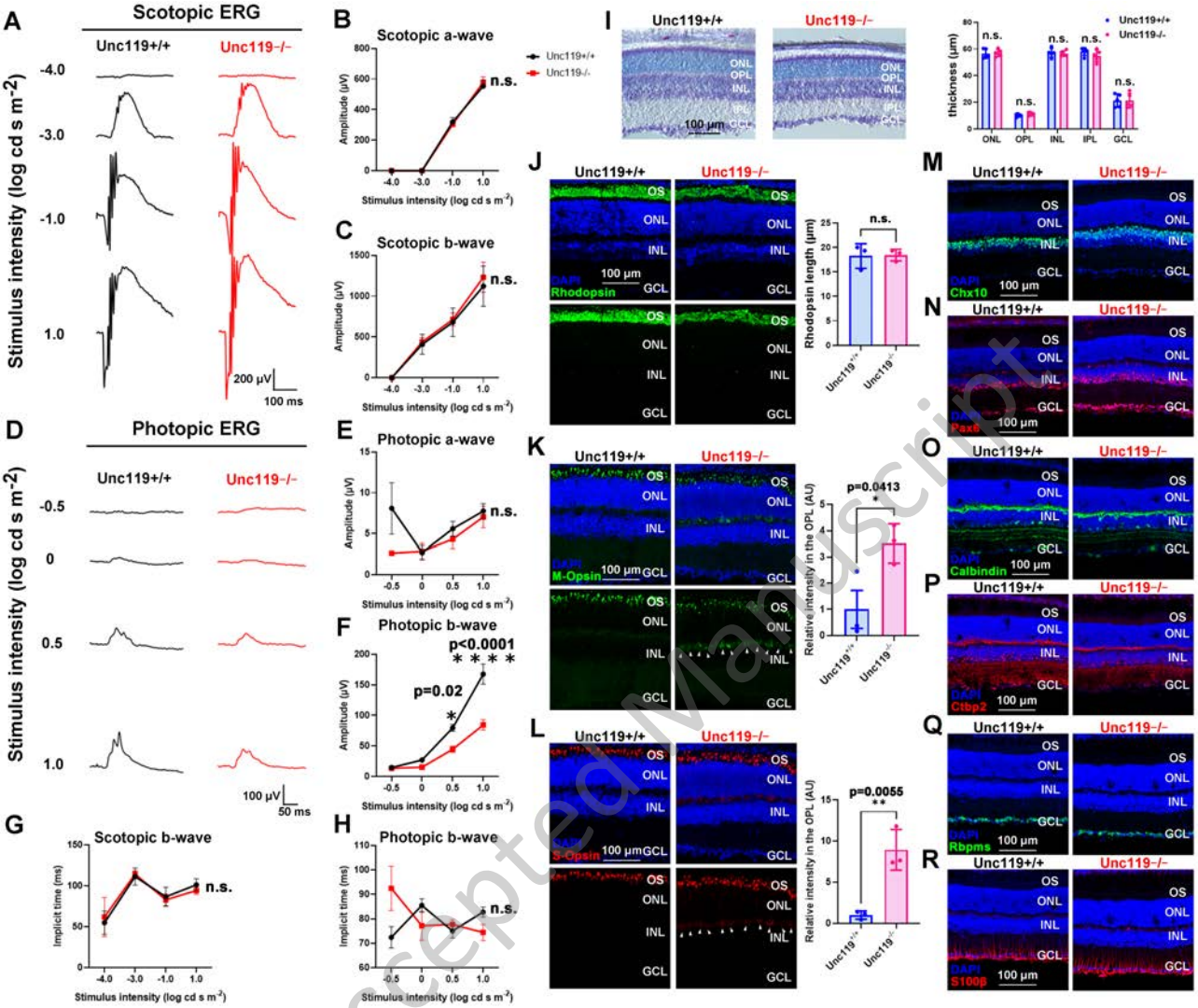

Figure 2

JNeurosci Accepted Manuscript

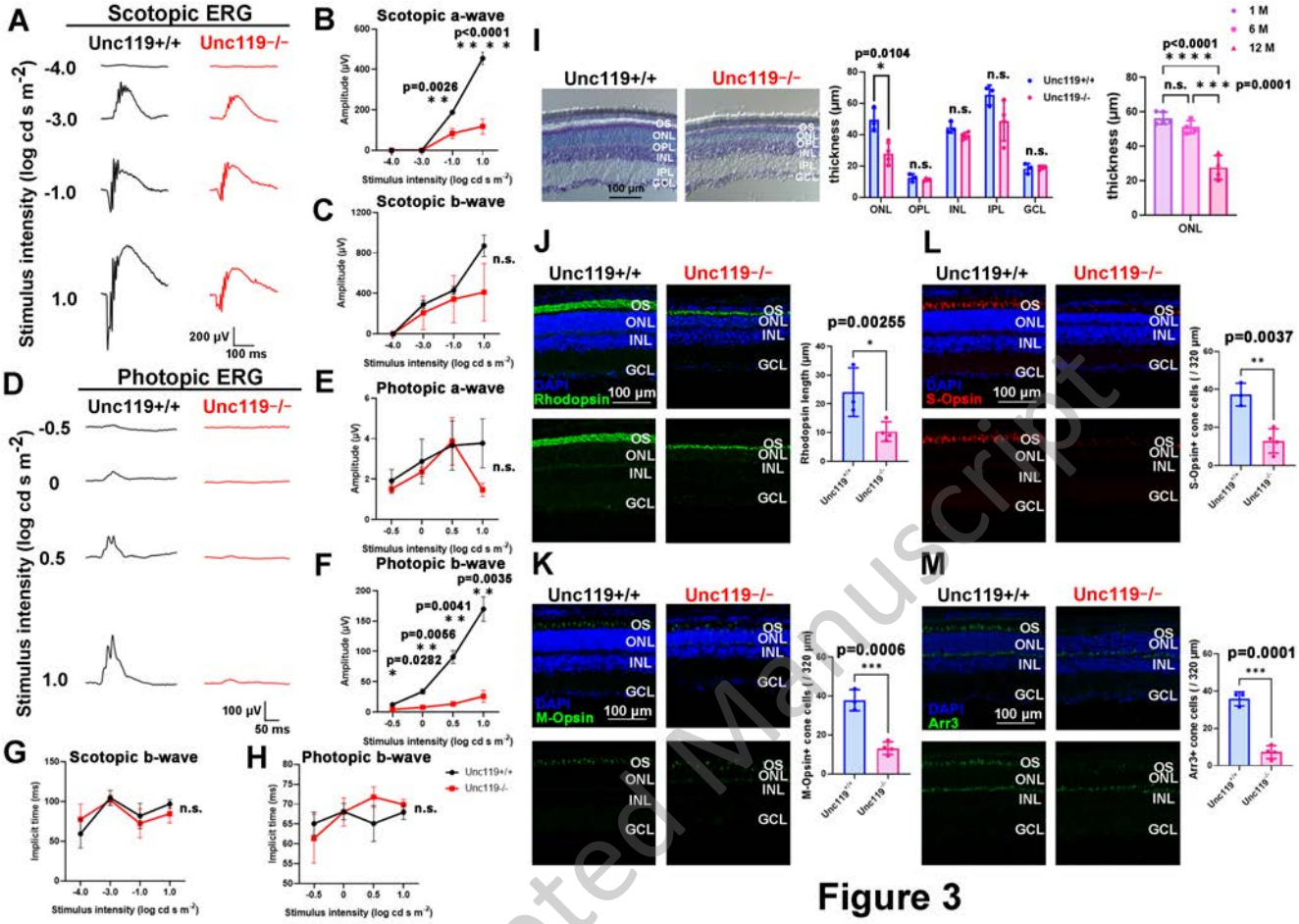

Figure 3

JNeurosci Accepted Manuscript

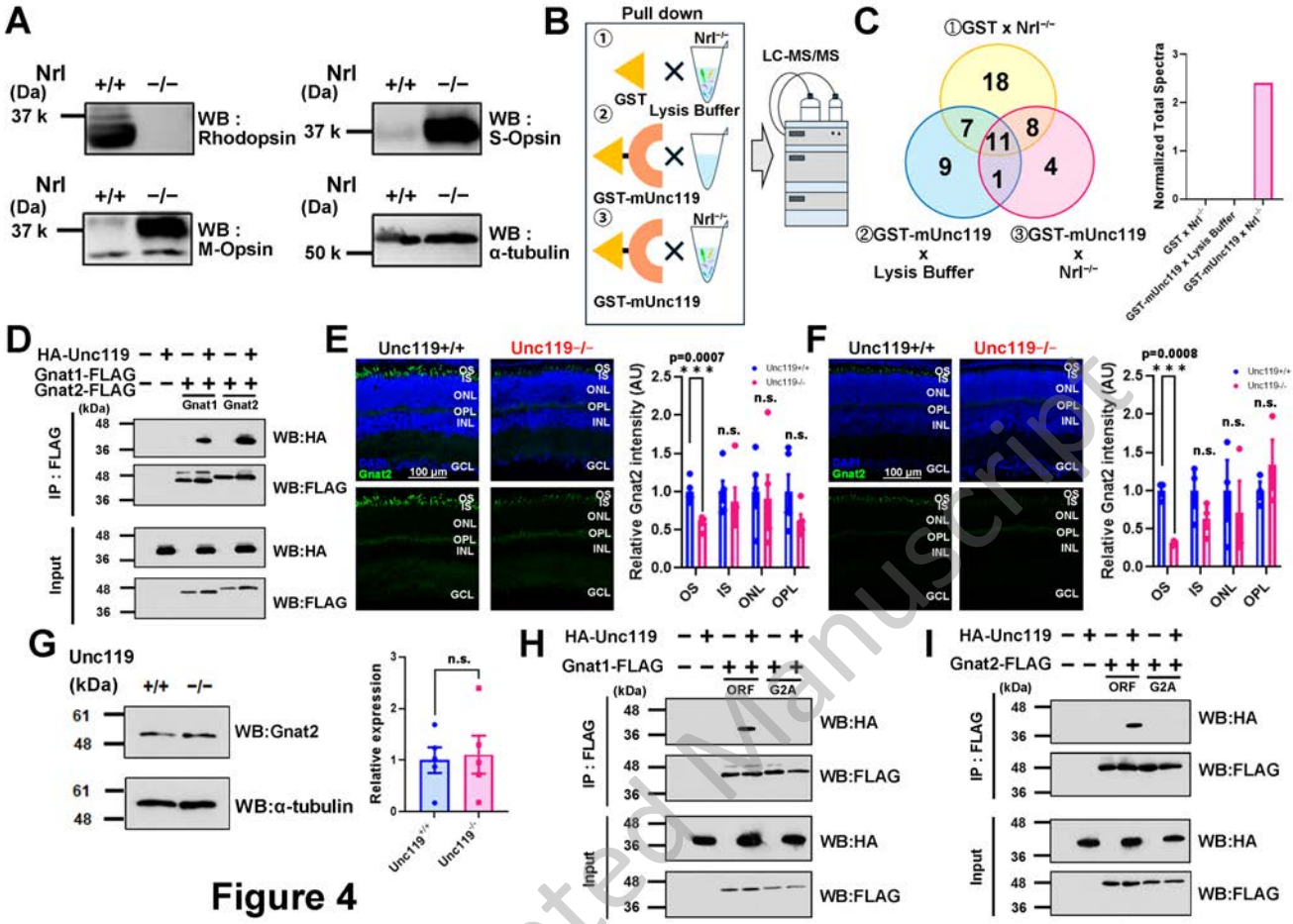

Figure 4

JNeurosci Accepted Manuscript

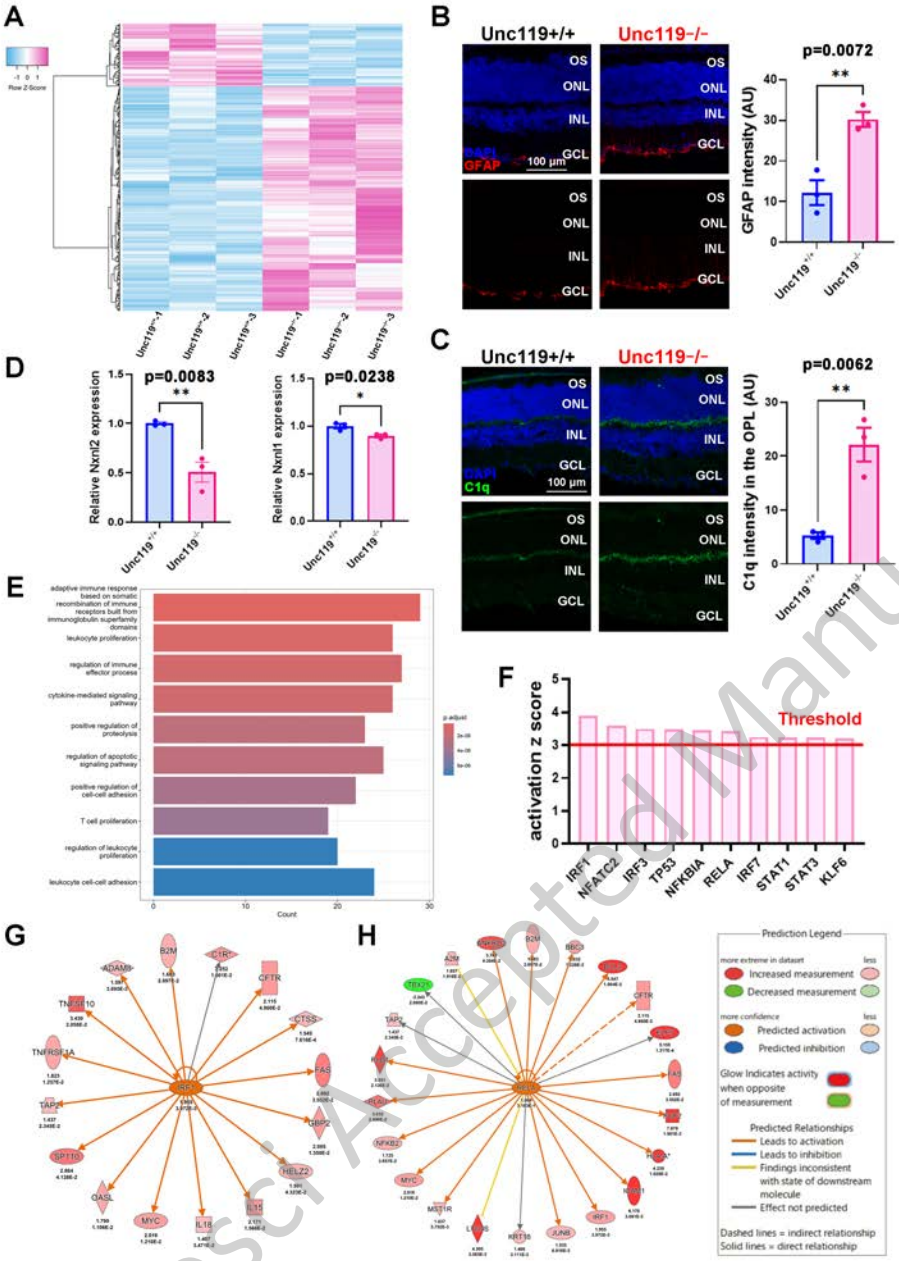

Figure 5

JNeurosci Accepted Manuscript

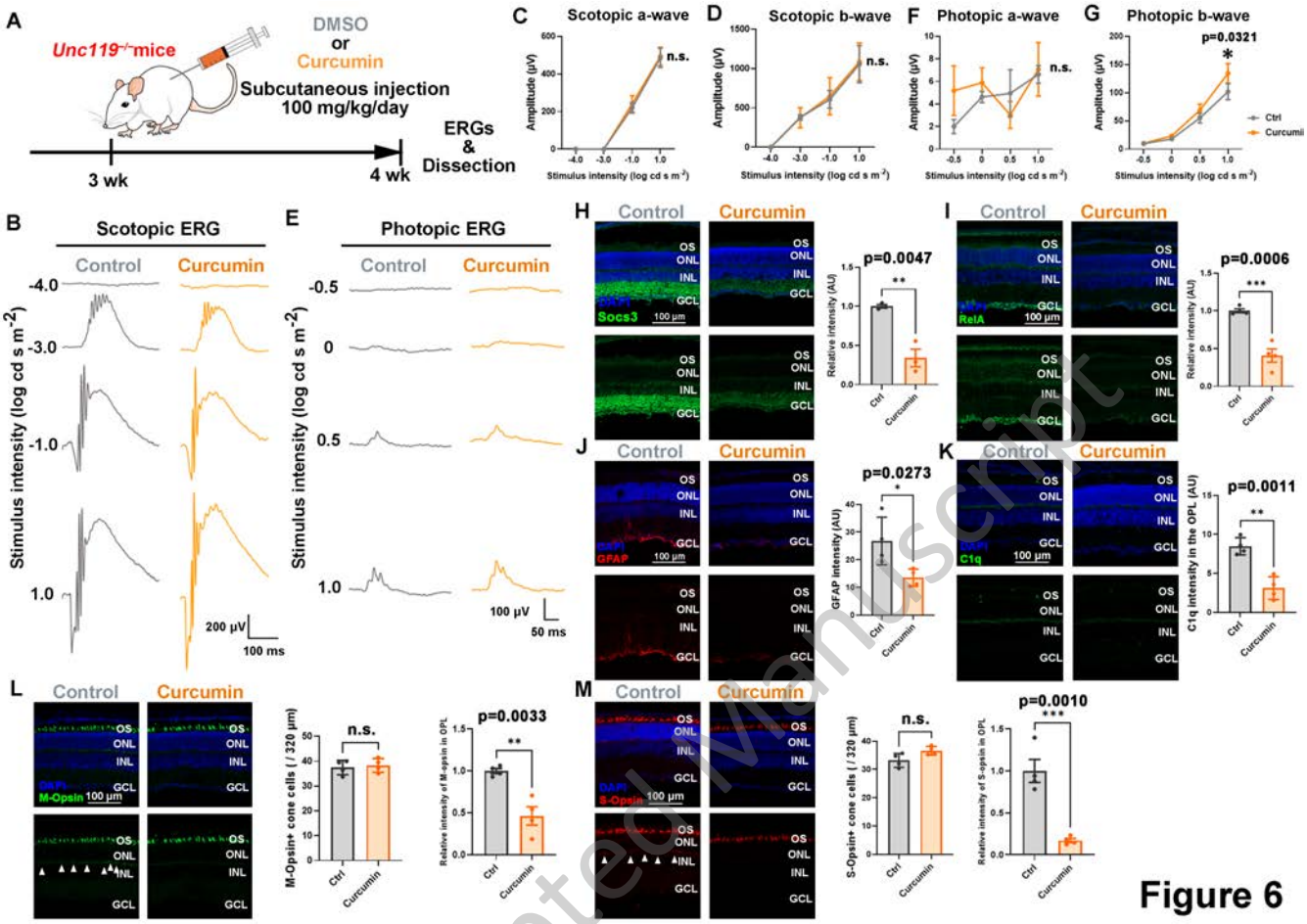

Figure 6

JNeurosci Accepted Manuscript

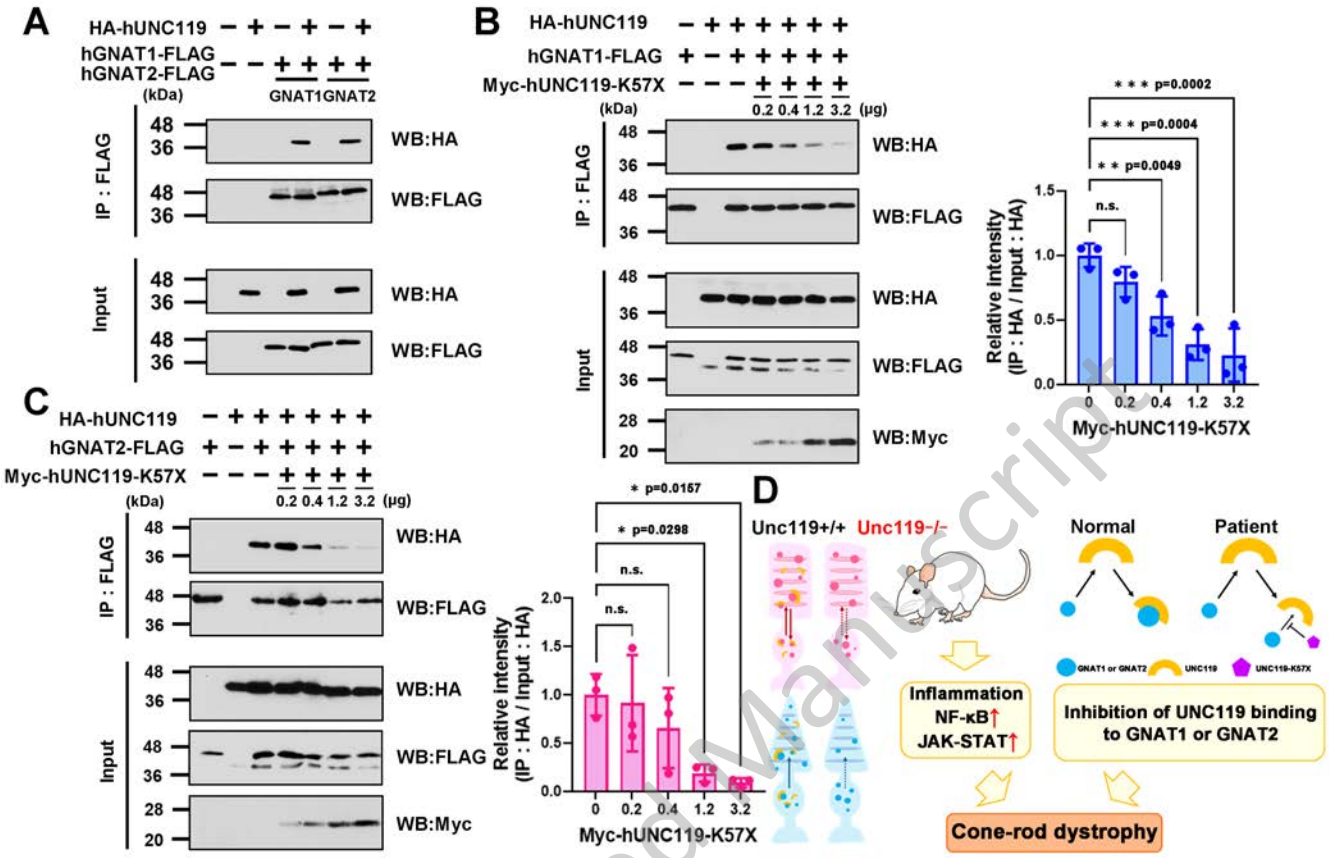

Figure 7

JNeurosci Accepted Manuscript